Annexure -VIII

UNIVERSITY GRANTS COMMISSION

BAHADUR SHAH ZAFAR MARG

NEW DELHI – 110 002.

Annual/Final Report of the work done on the Major Research Project.

(Report to be submitted within 6 weeks after completion of each year)

1. Project report No. 1st /2nd /3rd/Final **Final**

2. UGC Reference No.F. No. 43-520/2014/(SR) dated 16 - 10 - 2015

3. Period of report: from 01-07-2015 to 30-06-2018

4. Title of research project Quantum Phases of spin-1 bosonic atoms in Bichromatic Superlattices

5. (a) Name of the Principal Investigator Ramesh V Pai

(b) Deptt. Physics

(c) University/College where work has progressed **Goa University**

6. Effective date of starting of the project 01-07-2015

7. Grant approved and expenditure incurred during the period of the report:

a. Total amount approved Rs. Rs. 12,67,484.00

b. Total expenditure Rs. Rs. 12,02,494.00

c. Report of the work done: (Please attach a separate sheet)

Final Report Attached as Annexure A

i. Brief objective of the project

Develop cluster mean-field theory for 1, 2 and 3-dimensional spin-1 Bose-Hubbard model in BichromaticSuperlattices and study its phase diagram in detail, both at zero temperature and finite temperature.

ii. Work done so far and results achieved and publications, if any, resulting from the work (Give details of the papers and names of the journals in which it has been published or accepted for publication

OBJECTIVES WERE ACHIEVED:

1) Developed cluster mean-field theory to study the phase diagram of spin-1 Bose Hubbard models.

2) Obtained the phase diagram of Spin-1 Bose Hubbard model at zero and finite temperature.

3) Obtained the phase diagram of spin-1 Bose Hubbard model in bichromatic superlattice

ACHIEVEMENTS FROM THE PROJECT

1) Set up a Desktop based computer cluster for carrying out numerical calculations

2) Trained three research students to set up the computers laboratory and develop Fortran Programming.

3) Developed Cluster Mean field theory for Spin-1 Bose Hubbard model.

4) Studied the phase diagram of spin-1 Bose Hubbard model

iii. Has the progress been according to original plan of work and towards achieving the objective. if not, state reasons

Yes

iv. Please indicate the difficulties, if any, experienced in implementing the project_____

NIL

v. If project has not been completed, please indicate the approximate time by which it is likely to be completed. A summary of the work done for the period (Annual basis) may please be sent to the Commission on a separate sheet.

Project has been completed

vi. If the project has been completed, please enclose a summary of the findings of the study. One bound copy of the final report of work done may also be sent to University Grants Commission.

We apply the Cluster Mean Field Theory (CMFT) for 2-dimensional Spin-1 Bose-Hubbard model to account for the super fluid (SF)-Mott insulator (MI) transitions and characterize various magnetic phases that can arise in the presence of anti-ferromagnetic and the ferromagnetic interactions. CMFT calculations treat hopping of bosons within the cluster exactly, which allows us to study magnetic properties in all quantum phases. Our study yields Nematic behavior of super fluid and odd density

Mott insulator phases for anti-ferromagnetic interaction with a continues phase transition between them. Even density Mott insulator shows Nematic as well as singlet phase depending upon the strength of interaction and a continuous cross over between them. SF to singlet Mott insulator transition is discontinues. We also study the dependence of cluster size on the critical on-site interaction for the super fluid to Mott insulator transitions. For anti-ferromagnetic interaction critical on-site repulsion for SF-odd density MI transition increases with cluster size, however, no such change is observed for superfluid to singlet Mott insulator transition. In the case of ferromagnetic interaction super fluid to Mott insulator transitions are continues and we see an increase in the stability of Mott lobes as the cluster size grows. Using this cluster mean field theory formalism we also calculate quantum entanglement in various phases of this model by calculating second order Renyi Entanglement Entropy (EE), which can be directly measured in experiments. Calculated EE shows a large value in Nematic Mott insulator phase compared to all other phases.

Further we analyze superfluid, Mott insulator and various magnetic phases of ultracold spin-1 bosonic atoms in two-dimensional optical superlattices. Our studies have been performed using Cluster Mean Field Theory (CMFT). Calculations have been carried out for a wide range of densities and the energy shifts due to the superlattice potential. We find superlattice potential do not break the symmetry of the superfluid phases which is polar (ferro) superfluid for antiferromagnetic (ferromagnetic) interaction. Superlattice potentials induce Mott insulator phases with half-integer densities. The phase diagram is obtained using superfluid density, Nematic order and singlet density. Second order Rényi entanglement entropy (EE) is also calculated in different phases. The results show that Rényi EE is large in the Nematic MI phase.

vii. Any other information which would help in evaluation of work done on theproject. At the completion of the project, the first report should indicate the output, such as

(a)Manpower trained

Yes.

Ms. Chetana Ganesh FadteGaonker, project fellow joined for Ph. D

(b) Ph. D. awarded: Nil

(c) Publication of results

Two papers published.

1) Bhargav K Alavani, Ananya Das and Ramesh V Pai, Cluster mean field theory for two dimensional spin-1 Bose–Hubbard model,
J. Phys. B: At. Mol. Opt. Phys. 51 (2018) 145302.

2) Chetana G.F. Gaonker, B. K. Alavani, A. Das2 and R. V. Pai
Spin-1 Bosons in optical superlattice
Accepted for publication in AIP Conference Proceedings (2019).
Copies Attached

(d) other impact, if any

1) Trained man power for setting up computer cluster for parallel computation

2) Improved computational infrastructure at Goa University

**SIGNATURE OF THE PRINCIPAL INVESTIGATOR**

**REGISTRAR/PRINCIPAL**

**(Seal)**

# Annexure A

# Final Report

# Title: Quantum Phases of spin-1 bosonicatoms in Bichromatic Superlattices

## 1. Cluster Mean Field Theory applied to Spin-1 Bose Hubbard Model:Zero Temperature

### *1.1. Introduction*

In the experiments of optical lattice BEC of atoms is prepared in Magneto-Optical Traps (MOT) resulting in freezing of spin degrees of freedom. When traps are purely optical, Alkali atoms like $^{87}$Rb, $^{23}$Na and $^{30}$K having hyperfine spin $F = 1$, have spin degrees of freedom, and thus, the interaction between atoms is spin dependent. The interaction is ferromagnetic (e.g. $^{87}Rb$) or anti-ferromagnetic (e.g $^{23}Na$) depending upon scattering lengths of singlet and quintuplet channels[1]. This interaction not only modifies the nature of the phase diagram but also allows the study of superfluidity and magnetism.

A model which describes such spin full Bosons in an optical lattice is spin-1 Bose Hubbard Model defined by

$$\hat{H} = -J \sum_{\langle k,l\rangle,\sigma} (\hat{a}^{\dagger}_{k,\sigma}\hat{a}_{l,\sigma} + H.C) + \frac{U_0}{2}\sum_k \hat{n}_k(\hat{n}_k - 1) + \frac{U_2}{2}\sum_k (\vec{F}_k^2 - 2\hat{n_k}) - \mu\sum_k \hat{n}_k \quad (1)$$

where bosons with spin projection $\sigma = \{-1, 0, 1\}$ can hop between nearest neighboring pairs of site $\langle k, l\rangle$ with amplitude $J$, $\hat{a}^{\dagger}_{k,\sigma}(\hat{a}_{k,\sigma})$ is the boson creation (annihilation) operator for site $k$. Total number operator at site $k$ is $\hat{n}_k = \sum_\sigma \hat{n}_{k,\sigma}$ with $\hat{n}_{k,\sigma} = \hat{a}^{\dagger}_{k,\sigma}\hat{a}_{k,\sigma}$. $\vec{F}_k = (F^x_k, F^y_k, F^z_k)$ is the spin operator with $F^\alpha_k = \sum_{\sigma,\sigma'} \hat{a}^{\dagger}_{k,\sigma} S^\alpha_{\sigma,\sigma'} \hat{a}_{k,\sigma'}$ and $S^\alpha_{\sigma,\sigma'}$ are the standard spin-one matrices

$$S^x = \frac{1}{\sqrt{2}}\begin{pmatrix} 0 & 1 & 0 \\ 1 & 0 & 1 \\ 0 & 1 & 0 \end{pmatrix}, S^y = \frac{i}{\sqrt{2}}\begin{pmatrix} 0 & -1 & 0 \\ 1 & 0 & -1 \\ 0 & 1 & 0 \end{pmatrix} \text{ and } S^z = \begin{pmatrix} 1 & 0 & 0 \\ 0 & 0 & 0 \\ 0 & 0 & -1 \end{pmatrix}.$$

Using these matrices in the expression for $\vec{F}_k^2$, we get

$$\vec{F}_k^2 = \hat{n}_{k,1}^2 - 2\hat{n}_{k,1}\hat{n}_{k,-1} + \hat{n}_{k,-1}^2 + \hat{n}_{k,1} + \hat{n}_{k,-1} + 2\hat{n}_{k,0} + 2\hat{n}_{k,0}\hat{n}_{k,1} + 2\hat{n}_{k,0}\hat{n}_{k,-1} + 2\hat{a}_{k,1}^\dagger\hat{a}_{k,-1}^\dagger + 2\hat{a}_{k,0}^\dagger\hat{a}_{k,0}^\dagger\hat{a}_{k,1}\hat{a}_{k,0}. \quad (2)$$

The chemical potential $\mu$ controls the boson density. On-site interaction $U_0$ and $U_2$ arises due to the difference in the scattering lengths $a_0$ and $a_2$ of channels $S = 0$ and $S = 2$ respectively and are equal to $U_0 = 4\pi\hbar^2(a_0+2a_2)/3M$ and $U_2 = 4\pi\hbar^2(a_2-a_0)/3M$ where $M$ is a mass of the atom. For $^{23}Na$, $a_0 = 49.4a_B$ and $a_2 = 54.7a_B$ with $a_B$ as Bohr radius resulting $U_2 > 0$. Whereas for $^{87}Rb$, $a_0 = (110\pm4)a_B$ and $a_2 = (107\pm4)a_B$, so $U_2$ can be negative[1].

Various techniques like mean field methods [2, 3], variational Monte Carlo [4], analytical [5, 6], Density Matrix Renormalization Group (DMRG) for 1D[7, 8], and quantum Monte Carlo simulations in 1D [9] and 2D [10] have been used to study this model. Overall phase diagram at zero temperature shows the MI phase with each lattice site having commensurate boson filling when repulsion between atoms is large, and superfluid otherwise. The richness of the phases emerges due to their magnetic nature, and it depends on the sign and strength of spin-dependent interaction $U_2$. When the interaction is ferromagnetic, $U_2 < 0$, the superfluid to Mott insulator transition is continuous. However, for anti-ferromagnetic interactions, $U_2 > 0$, the even density Mott insulator phase is found to be more stable than the odd density Mott insulator phase. The superfluid phase is polar in nature and transition to even density Mott insulator phase is discontinuous due to singlet formation. Mott phase has nematic behavior and a weakly first-order transition to singlet state is predicted in even density Mott insulator.

Quantum Entanglement[11], an intrinsic phenomenon, plays a vital role in the quantum phase transitions and can be characterized by calculating bipartite Entanglement Entropy(EE)[12]. Methods like exact diagonalization[13, 14], density matrix renormalization group[15, 16], time-evolving block decimation [17], the slave-boson approach [18], and Monte Carlo simulation [19] have been used to calculate the von Neumann entropy (i.e., first -order Rényi EE) and the Rényi EE to second-order in various BH systems. Recently Rényi Entanglement Entropy has been experimentally measured to characterize SF-MI transitions in the case of spinless bosons[20].

Single site mean field theory, numerically elementary when applied to spin-1 Bose Hubbard model [3] predicts primary phase diagrams correctly. But it fails to predict the magnetic nature of the different phases and calculate Entanglement Entropy. It is also known to overestimate the critical interaction for superfluid to Mott insulator transition. It is so desired to have a procedure which keeps the simplicity of the mean field theory but overcome some of its limitations. One such method is the cluster mean field theory [21], which has been widely used to study phase transitions in various BH models[22, 20]. This method concentrates on a cluster of sites rather than a single site, forming a bridge between simple mean field theory and heavy numerical methods like DMRG and Monte Carlo simulations.

Below we apply the cluster mean field theory to the spin-1 Bose Hubbard Model to account for the different phases that originate due to ferromagnetic and anti-ferromagnetic interactions and then, obtain the phase diagram for the $2D$ system. Also, use this CMFT formalism to get the signature of Rényi EE to SF-MI transition in this model. The CMFT formalism for the Spin-1 BH model is given in the next section, followed by results and conclusions.

### *1.2. Model and cluster mean-field formalism*

In the cluster mean-field framework, we partitioned the lattice into clusters with $N_C$ number of sites each. Decoupling the clusters from its neighbours using standard mean field decoupling scheme i.e., $\hat{a}^\dagger_{k,\sigma}\hat{a}_{l,\sigma} + \hat{a}_{k,\sigma}\hat{a}^\dagger_{l,\sigma} \approx \hat{a}^\dagger_{k,\sigma}\psi_{l,\sigma} + \hat{a}_{k,\sigma}\psi^*_{l,\sigma} - \psi^*_{k,\sigma}\psi_{l,\sigma} + \hat{a}^\dagger_{l,\sigma}\psi_{k,\sigma} + \hat{a}_{l,\sigma}\psi^*_{k,\sigma} - \psi^*_{l,\sigma}\psi_{k,\sigma}$ where $\psi_{k,\sigma} = \langle\hat{a}_{k,\sigma}\rangle$ represents the superfluid order parameter with spin components $\sigma$ result Hamiltonian (1) is given by

$$\hat{H} = \sum_{cluster} \hat{H}^{cluster} \tag{3}$$

where

$$\begin{aligned}\hat{H}^{cluster} = &-J \sum_{<k,l>,\sigma}^{N_c} (\hat{a}^\dagger_{k,\sigma}\hat{a}_{l,\sigma} + H.C) + \frac{U_0}{2}\sum_{k}^{N_c}\hat{n}_k(\hat{n}_k - 1) \\ &+ \frac{U_2}{2}\sum_{k}^{N_c}(\hat{F}^2_k - 2\hat{n_k}) - \mu\sum_{k}^{N_c}\hat{n}_k \\ &- t\sum_{k,\sigma}^{N_c}\sum_{l}{}'(\hat{a}^\dagger_{k,\sigma}\psi_{l,\sigma} + \hat{a}_{k,\sigma}\psi^*_{l,\sigma} - \psi^*_{k,\sigma}\psi_{l,\sigma}),\end{aligned} \tag{4}$$

where in $\sum'_l$, $l$ runs over all sites which are nearest neighbor to site $k$ and belongs to neighboring clusters. We set the energy scale by choosing $J = 1$, as a result, all the physical parameters considered are dimensionless. This Hamiltonian is solved self consistently for the values of $\psi_{k,\sigma}$ using the following procedures. Assuming initial values for the $\psi_{i,\sigma}$ we first construct the Hamiltonian matrix in Fock's state basis $|\{N_{1,\sigma}\};\{N_{2,\sigma}\};...;\{N_{C,\sigma}\}\rangle \equiv |\{N_1\rangle\} \otimes \{|N_2\rangle\} \otimes ..., \{|N_C\rangle\}$. Here $|\{N_i\}\rangle \equiv |N_{i,-1}, N_{i,0}, N_{i,1}\rangle$ with $N_{i,\sigma}$ representing the number of bosons with spin component $\sigma$ at site $i$. We assumes values $N_{i,-1} + N_{i,0} + N_{i,1} = 0, 1, 2, ..., N_{max}$ where $N_{max}$ is chosen sufficiently large so that ground state energy is properly converged. We then diagonalize Hamiltonian matrix to obtain the ground state energy and the wave function given by $|\Psi_{GS}\rangle = \sum_{N_1;N_2;...;N_C}^{N_{max}} C_{N_1,N_2,...,N_C}|N_1, N_2, ..., N_C\rangle$. We calculate $\psi_{i,\sigma} = \langle\Psi_{GS}|\hat{a}_{i,\sigma}|\Psi_{GS}\rangle$ and solve it self consistently. Homogeneity of lattice makes $\psi_{i,\sigma} \equiv \psi_\sigma$ independent of lattice site. For the superfluid phase at least one value of $\psi_\sigma$ is non zero; whereas for Mott Insulator phase all components are zero and shows density $\rho = \sum_\sigma\langle\hat{n}_\sigma\rangle$ as an integer. Superfluid density is given by $\rho_{SF} = \sum_\sigma|\psi_\sigma|^2$.

The magnetic properties of different phases of model (1) are studied by calculating the local magnetic moment identifier $\langle F^2 \rangle$ at a site [1] and the global (or cluster) magnetic moment identifier $\langle F^2_{TOT} \rangle = \langle \left( \sum_k^{N_C} F_k \right)^2 \rangle$ . Order parameter which characterizes Nematic order is

$$Q_{k,\alpha,\alpha} = \langle \hat{F}^2_{k,\alpha,\alpha} - \frac{1}{3} \hat{F}^2_k \rangle \tag{5}$$

where $(\alpha = x, y, z)$. Spin isotropy exists if $Q_{\alpha,\alpha} = 0$ for all $\alpha$ and indicate spin anisotropy (characteristic of the nematic order) if $Q_{\alpha,\alpha} \neq 0$. When the spin dependent interaction is antiferromagnetic, the density of singlet pair is given by $\rho_{SD} = \langle \hat{A}^\dagger_{SD} \hat{A}_{SD} \rangle$ where singlet creation operator $A^\dagger_{SD} = \frac{1}{\sqrt{6}} (2a^\dagger_1 a^\dagger_{-1} - a^\dagger_0 a^\dagger_0)$. In this study, we choose cluster sizes of $N_C = 1, 2$ and 4 as shown in Fig. 1 for obtaining the phase diagram.

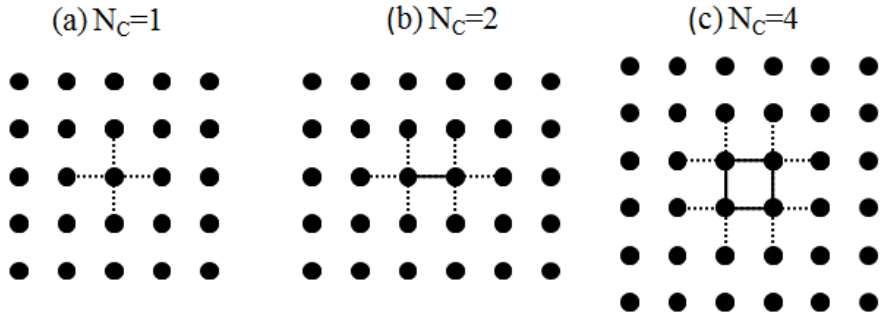


**Figure 1.** Clusters of sizes (a) $N_C = 1$, (b) $N_C = 2$ and (c) $N_C = 4$ used for obtaining the phase diagrams given in Figs. 5 and 8(d). Black solid circles represent sites, with dashed black lines as hopping of bosons outside cluster approximated using mean field decoupling. Solid Back lines represent hopping within the cluster treated exactly.

To obtain a signature of the quantum entanglement in various phases of this model, we calculate bipartite Entanglement Entropy(EE)[12]. Rényi EE is a bipartite entanglement defined by separating the whole system into two subsystems, and its second-order form can be measured in experiments. Denoting the two subsystems as A and B, the $n^{th}$-order Rényi EE is defined as

$$S_n[A(B)] = \frac{1}{1-n} log[Tr(\hat{\rho}^n_{A(B)})], \tag{6}$$

where $\hat{\rho}^n_{A(B)} = Tr_{B(A)}(\hat{\rho}_{AB})$ is the reduced density matrix of subsystem $A(B)$ and $\hat{\rho}_{AB}$ is the density matrix of the whole system. If the two subsystems are entangled, ignoring information about one subsystem will result in the other subsystem is being in a mixed quantum state. In our work here we concentrate on the second order $n = 2$ Rényi EE, $S_2[A(B)] = -log[Tr(\rho^2_{A(B)})]$.

In our cluster mean field treatment, intra-cluster correlations are reserved, and we consider intra-cluster bipartite entanglement. We calculate this for a cluster size of $N_C = 2$ to keep both the subsystems consisting of a single site. If subsystem $A$ is one of

the two sites, then subsystem $B$ is the remaining site. Therefore, the reduced density matrix for the site $A$ is $\rho_A = \sum_{N_1 N_1'} (\sum_{N_2} C^*_{N_1,N_2} C_{N_1',N_2}) |N_1\rangle\langle N_1'|$, and we calculate the second-order Rényi EE $S_2$ for different parameters. Results obtained for both $U_2 > 0$ and $U_2 < 0$ are given below in subsections 1.3 and 1.4 respectively.

### *1.3. Results:Antiferromagnetic case:* $U_2 > 0$

We first consider the anti-ferromagnetic case $U_2 > 0$. Here the superfluid phase is polar (PSF) which has symmetry $[U(1) \times S_2]/Z_2$ [3]. Since we have assumed $\psi_\sigma$ to be real, above symmetry allows $\psi_\sigma$ only two possible set of values $(i)$ $\psi_1 = \psi_{-1} \neq 0,\ \psi_0 = 0$ or $(ii)$ $\psi_1 = \psi_{-1} = 0,\ \psi_0 \neq 0$. This behaviour is evident from the figure 2(a) where we plot SF order parameters $\psi_\sigma$ and boson densities $\rho_\sigma$ as a function of chemical potential $\mu$ with $N_C = 2$ for the on-site interactions $U_0 = 21.8$ and $U_2 = 0.03U_0$. From this figure, we infer that superfluidity for these parameters is primarily due to bosons with spin component $\sigma = \pm 1$. In the Fig. 2(b), we plot SF density $\rho_{SF}$ and total boson density $\rho$ for the same set of parameters showing the transition from (SF where $\rho_{SF} \neq 0$) to a MI (where $\rho_{SF} = 0$ and $\rho = 1, 2$) phase. The SF to $\rho = 2$ MI transition is discontinuous, whereas SF - $\rho = 1$ MI transition shows very weak discontinuity. To understand the discontinuity across SF - MI($\rho$=1) transition, we plot, in Fig. 3, the ground state energy as function of SF order parameter $\psi_\pm$ near the SF - MI($\rho$=1) transition for different cluster sizes. Since $\psi_0 = 0$ in the polar superfluid phase, the ground state energy $E_0$ is a function of $\psi_\pm$. The single site mean-field theory shows two symmetric energy minima in the energy function yielding a continuous SF to MI transition. However, we observe a small third minimum in the cluster mean-field theory calculations with cluster sizes 2 and 4 which represent weakly first order transition.

In the Fig. 2(c), we plot singlet pair density $\rho_{SD}$, nematic order parameter $Q_{ZZ}$, local magnetic moment identifier $\langle F^2 \rangle$, and global magnetic moment identifier $\langle F^2_{TOT} \rangle$. Formation of singlets pairs commences when boson density $\rho$ is more than one and increases as we reach to $\rho = 2$ MI phase. There is precisely one singlet pair at each site in $\rho = 2$ MI phase. Further increase of $\mu$, superfluid nature of bosons suppresses singlet pair formation initially, however, increases with density $\rho$. The nematic order parameter is finite everywhere except in the $\rho = 2$ MI singlet phase. The global magnetic moment is seen to be nonzero in the SF phase while it is zero in MI phases. The local magnetic moment is zero in $\rho = 2$ MI phase due to singlet formation. Figure 2(d) shows the calculated EE in SF and MI phases. This result indicates that the nematic MI has large EE compared to all other phases. This observation can be understood as follows. Even though bosons are localized in the MI phase, weak quantum mechanical tunneling is possible to the nearby sites which are captured in the CMFT formalism, and due to the antiferromagnetic interaction at a site, the cluster tends to minimize its total magnetic moment. Because of this, each site is non-locally entangled with the nearby sites resulting in a high EE. The calculated EE also shows discontinuity as one goes from SF to the MI phase.

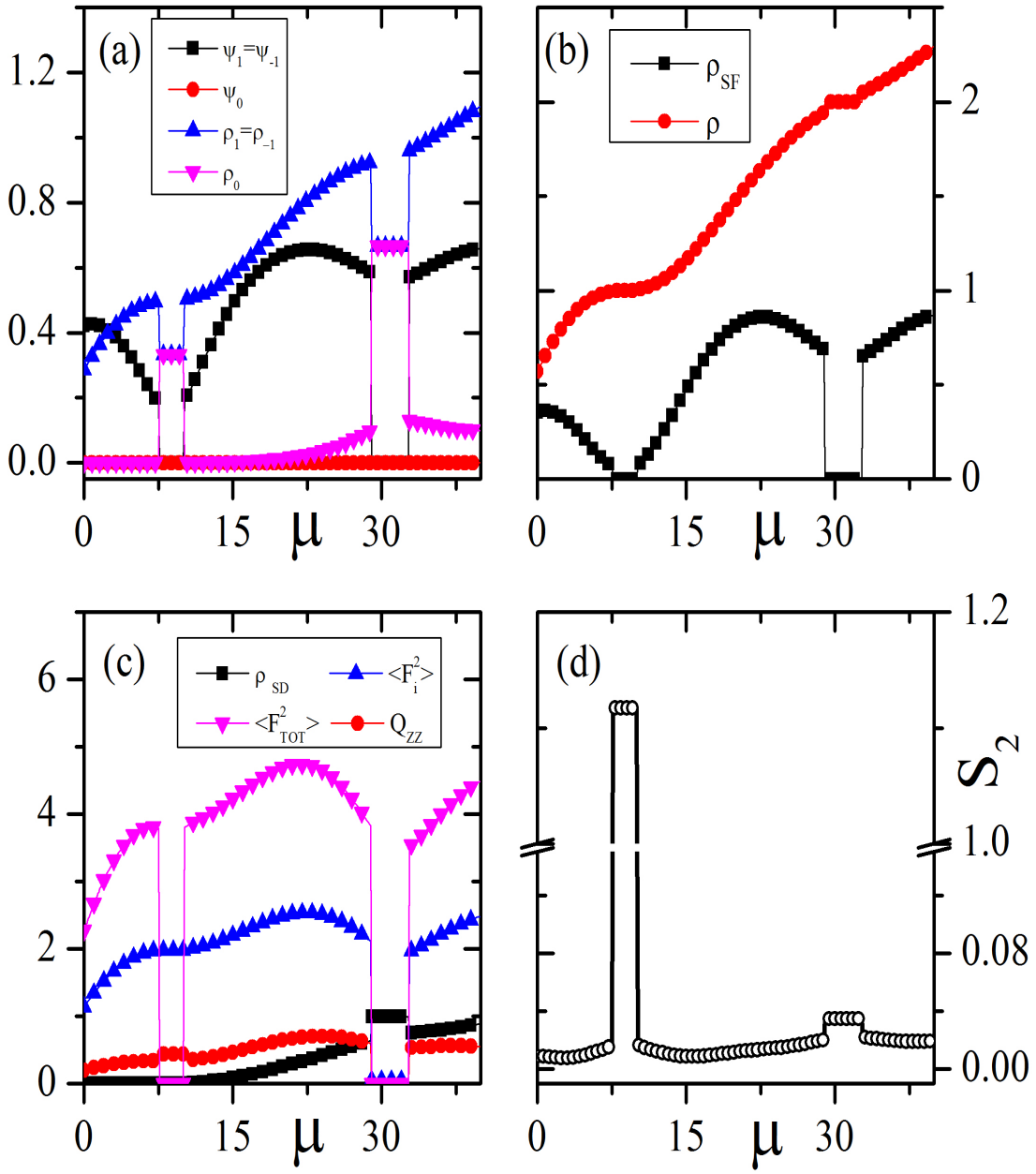


**Figure 2.** Plot of (a) superfluid order parameters $\psi_\sigma$, their boson densities $\rho_\sigma$, (b) superfluid density $\rho_{SF}$, boson density $\rho$, (c) Singlet pair density $\rho_{SD}$, nematic order parameter $Q_{ZZ}$, local magnetic moment $\langle F^2 \rangle$, global magnetic moment $\langle F^2_{TOT} \rangle$ identifiers, and (d) Entanglement Entropy $S_2$ for $U_2 = 0.03\ U_0$ and $U_0 = 21.8$ with $N_C = 2$.

The superfluid density is plotted as a function of chemical potential $\mu$ in Fig. 4, for cluster sizes $N_C = 1, 2$ and 4 for $U_0 = 21.8, U_2 = 0.03U_0$. With an increase in

the cluster size, the SF density decrease. Also, there is no MI phase predicted in the calculations when $N_C = 1$. However, when $N_C = 2$ and 4, the fluctuations neglected in the calculation with $N_C = 1$, are included and pushes the system to the MI phases. The MI phases correspond to the range of $\mu$ values for which the superfluid density vanishes. We analyze similar plots for different values of $U_0$ to yield the phase diagram plotted in Fig. 5. As the cluster size increases, the critical onsite interaction $U_0^C$ for the SF-MI transition decreases, which are more significant for SF-Nematic MI phase transition compares to SF-singlet MI transition. The single site mean-field calculations overestimate the superfluidity.

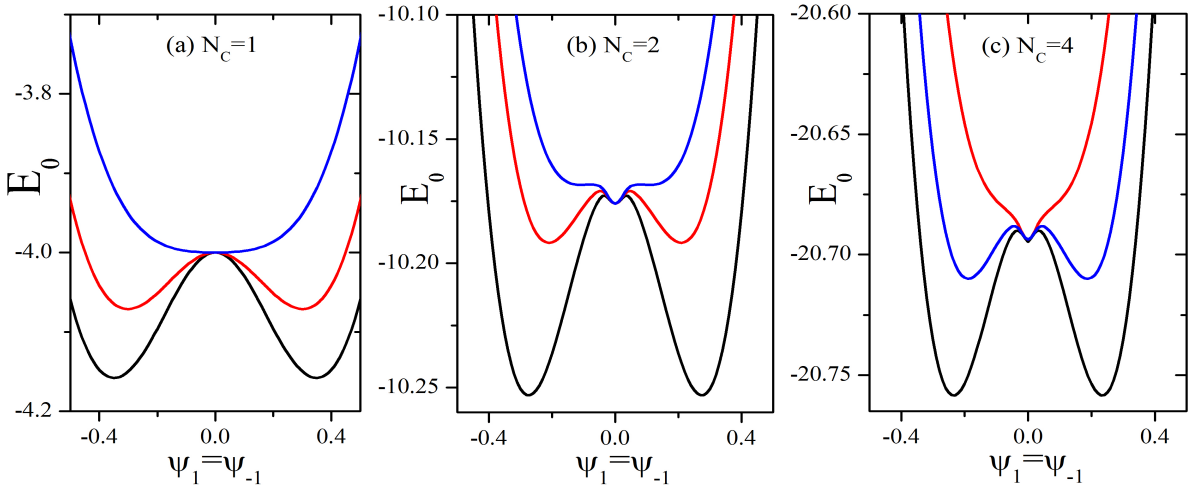


**Figure 3.** Ground state energies $E_0$ against SF order parameters $\psi_{-1} = \psi_1, \psi_0 = 0$ near SF-$\rho = 1$ MI transition for (a) $N_C = 1$, (b) $N_C = 2$ and (c) $N_C = 4$.

Another advantage of using CMFT is seen from Fig. 6 where we choose values of $U_0$ and $\mu$ in the deep $\rho = 2$ MI phase and plot singlet pair density $\rho_{SD}$, nematic order parameter $Q_{ZZ}$, local magnetic moment identifier $\langle F_i^2 \rangle$, and global magnetic moment identifier $\langle F_{TOT}^2 \rangle$ for different $U_2/U_0 > 0$ for $N_C = 1,\ 2$ and 4. Single site mean-field theory shows complete singlet formation for all values of $U_2/U_0$, whereas CMFT results show that for small values of interaction $U_2/U_0$ nematic phase is preferred. As $U_2$ increases, singlet formation grows, and the nematic behavior vanishes. Similar behavior is also seen for $\langle F^2 \rangle$ and $\langle F_{TOT}^2 \rangle$. In single-site MFT, a site is decoupled from its neighbors and for MI phase has all $\psi_\sigma = 0$, the tunneling of bosons to nearest sites is fully cut off yielding singlet state for all $U_2/U_0$. However, in CMFT, weak tunneling of bosons inside the cluster favors nematic order for small $U_2/U_0$. This crossover between nematic to singlet phase in $\rho = 2$ MI phase is first observed in the quantum Monte-Carlo simulations [10].

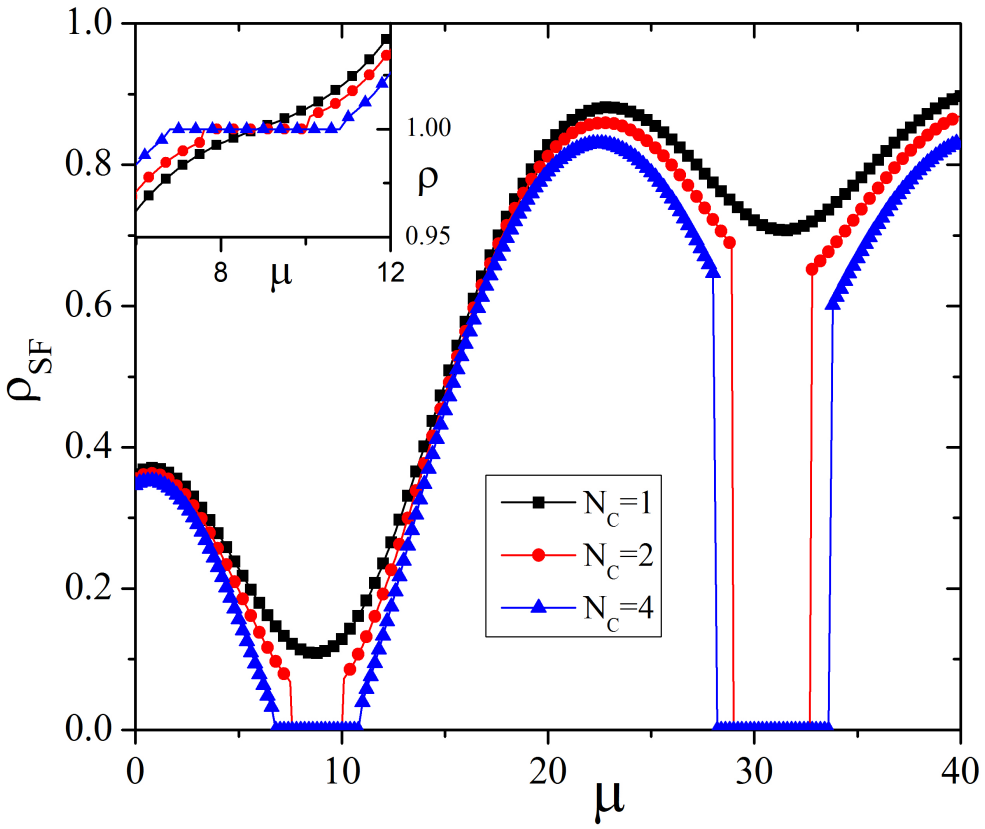


**Figure 4.** SF density $\rho_{SF}$ as a function of chemical potential $\mu$ for different values of cluster size $N_C$. (inset) Boson density $\rho$ as function of chemical potential $\mu$ near unit density.

### *1.4. Results:Ferromagnetic case:* $U_2 < 0$

We perform a similar calculation for the case $U_2 < 0$. Here the superfluid phase is ferromagnetic(FSF) and has an order parameter manifold with symmetry group $SO(3)$. Assuming the superfluid order parameter to be real, we get $\psi_1 = \psi_{-1} \neq 0, \psi_0 = \sqrt{2}\psi_1$ [3].

Figure 7(a) shows superfluid order parameters for $U_2/U_0 = -0.03, U_0 = 40$ with $N_C = 2$. Here superfluidity is due to all spin components. In figure 7(b) the SF density $\rho_{SF}$ and the total boson density $\rho$ are plotted for the same set of parameters. We find the transition from the FSF to MI phase is continuous. In figure 7(c) local magnetic moment identifier $\langle F^2 \rangle$, nematic order parameter $Q_{ZZ}$, and local magnetic moment identifier $\langle F^2_{TOT} \rangle$ are plotted. The nematic order parameter is seen to be finite in FSF and MI phases due to its magnetic nature. The global magnetic moment and the local magnetic moment is maximized in FSF as well as in MI phases due to on-site ferromagnetic interactions. Figure 2(d) shows the calculated EE in FSF and MI phases.

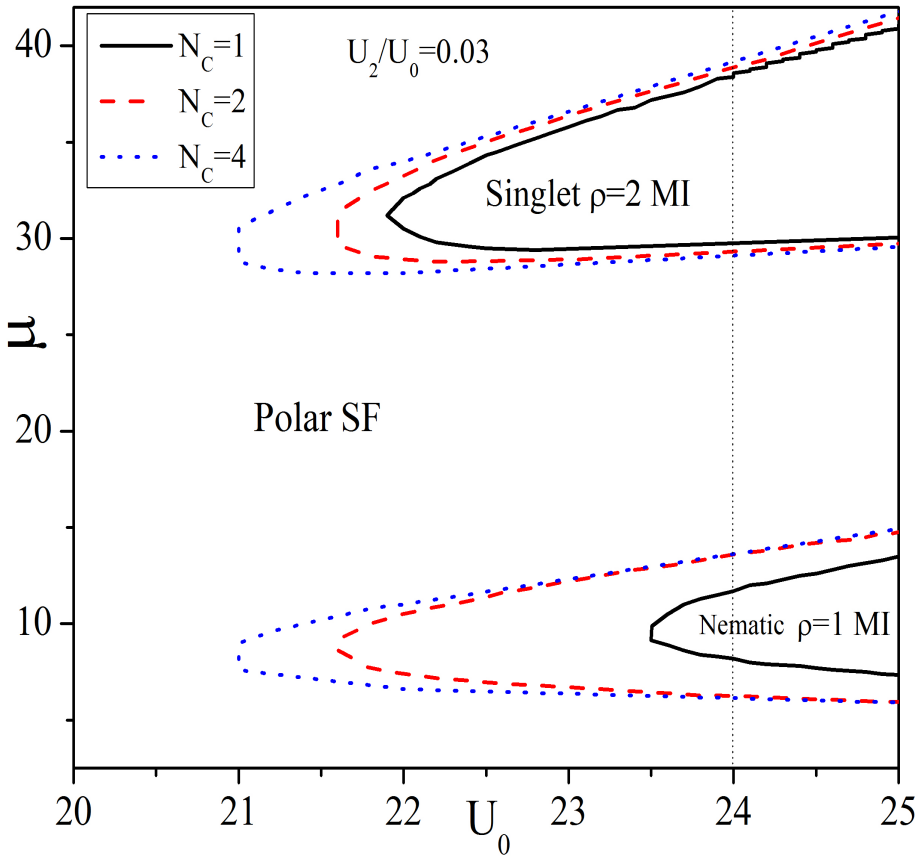


**Figure 5.** Phase diagram for $U_2 = 0.03\ U_0$ obtained for different cluster size $N_C$. As $N_C$ increases both $\rho = 1$ and 2 MI lobes enlarge reducing critical $U_0^C$.

The EE $S_2$ is continuous but shows a discontinuity in its first derivative as one goes from FSF to Ferro MI phase.

We plot superfluid density for different cluster sizes in Fig. 8(a) and (c). Since the Ferro SF to MI transitions is continuous as seen from these figures, the fluctuations play an important role near the phase boundaries. The superfluid density is reduced due to these fluctuations and leads to observed enlargement of Mott lobes with cluster size. In Fig. 8(b) and (d) we plot the phase diagrams for different cluster sizes.

The calculated critical value of $U_0^C$ are given in the Table 1 for both $U_2 > 0$ and $U_2 < 0$. Spin dependent on site interaction is kept $|U_2| = 0.03U_0$. The critical $U_0^C$ decreasing with increasing $N_C$.

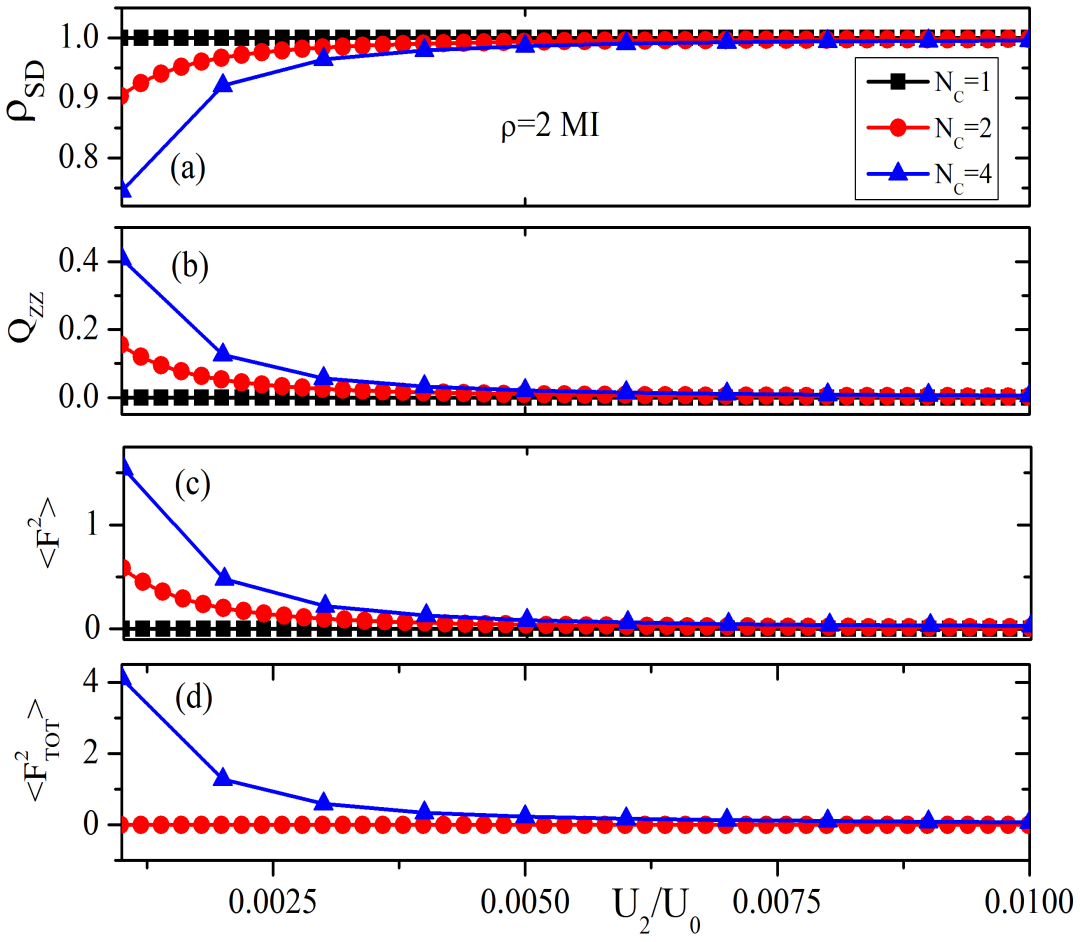


**Figure 6.** Plot of singlet density $\rho_{SD}$, nematic order parameter $Q_{ZZ}$, local magnetic moment $\langle F^2 \rangle$, and global magnetic moment $\langle F^2_{TOT} \rangle$ in $\rho = 2$ MI phase for varying $U_2/U_0$ for $N_C = 1$, 2 and 4. Single site mean-field calculations show complete singlet formation for all $U_2/U_0 > 0$ values . However, CMFT shows nematic behaviour for low values of $U_2/U_0$ and as the interaction strength increases Mott phase cross over to singlet phase.

| $N_C$ | $U_0^C(\pm 0.1)$ for $U_2 > 0$ | | $U_0^C(\pm 0.1)$ for $U_2 < 0$ | |
|---|---|---|---|---|
| | $(\rho = 1)$ PSF-MI | $(\rho = 2)$ PSF-MI | $(\rho = 1)$ FSF-MI | $(\rho = 2)$ FSF-MI |
| 1 | 23.4 | 21.9 | 24.2 | 40.9 |
| 2 | 21.7 | 21.6 | 23.1 | 39.0 |
| 4 | 21.1 | 21.0 | 21.8 | 36.7 |

**Table 1.** Critical values of $U_0$ for different $N_C$

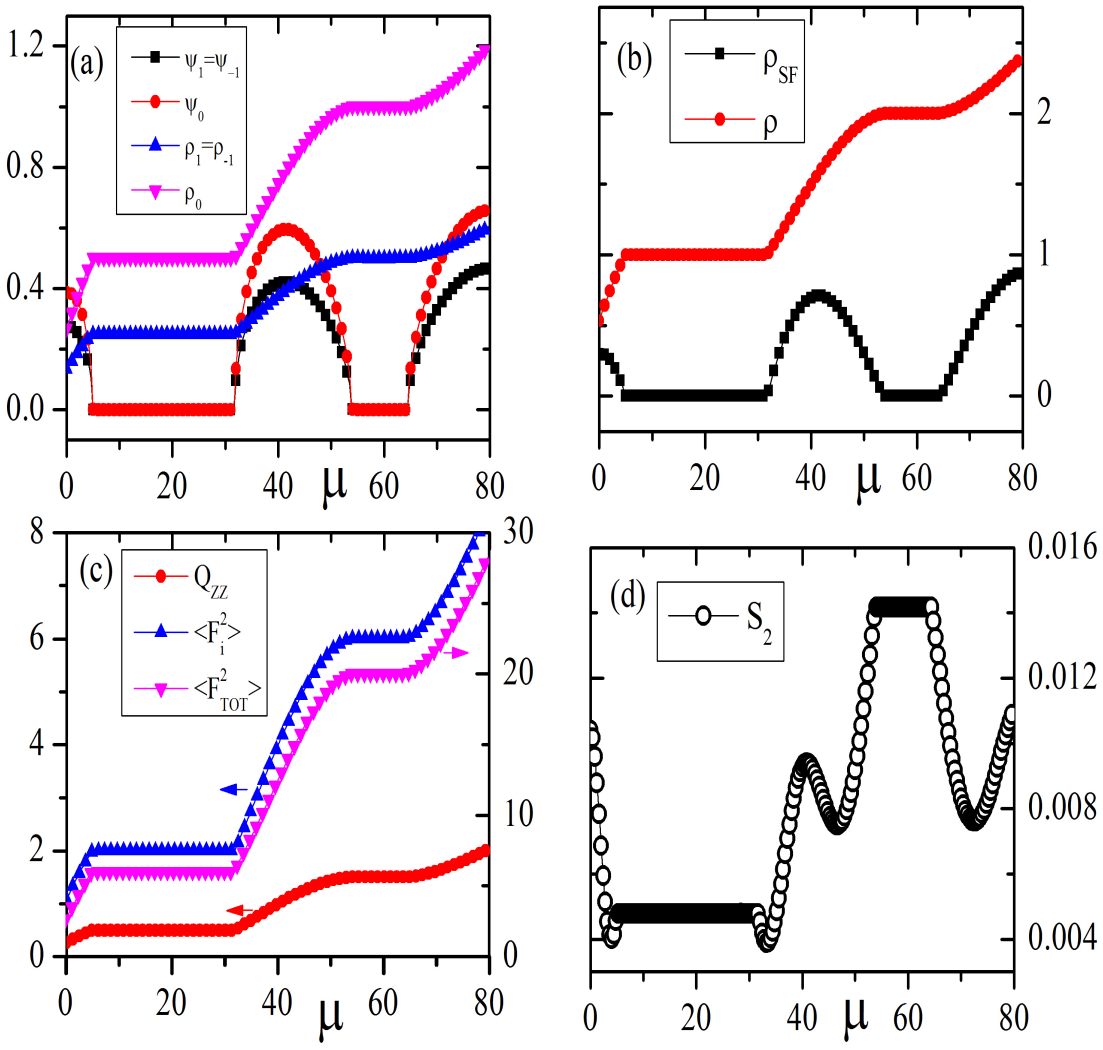


**Figure 7.** Plots of (a) superfluid order parameters $\psi_\sigma$, their boson densities $\rho_\sigma$ (b) superfluid density $\rho_{SF}$, boson density $\rho$ (c) nematic order parameter $Q_{ZZ}$, local magnetic moment $\langle F^2 \rangle$, global magnetic moment $\langle F^2_{TOT} \rangle$, and (d) Entanglement Entropy $S_2$ for $U_2 = -0.03\ U_0$ and $U_0 = 40$ with $N_C = 2$.

### *1.5. Conclusion*

In this chapter, cluster mean-field theory is generalized for the spin-1 Bose-Hubbard model to study various phases and phase transitions possible in the spin-1 BH model. In this calculation, we consider cluster size up to 4 sites, and density $\rho \leq 3$. Treating the tunneling between the sites inside a cluster exactly, CMFT allows studying magnetic phases in addition to superfluid and Mott insulator phases. For anti-ferromagnetic interaction ($U_0 > 0$), the superfluid phase is polar, odd density Mott insulator is nematic

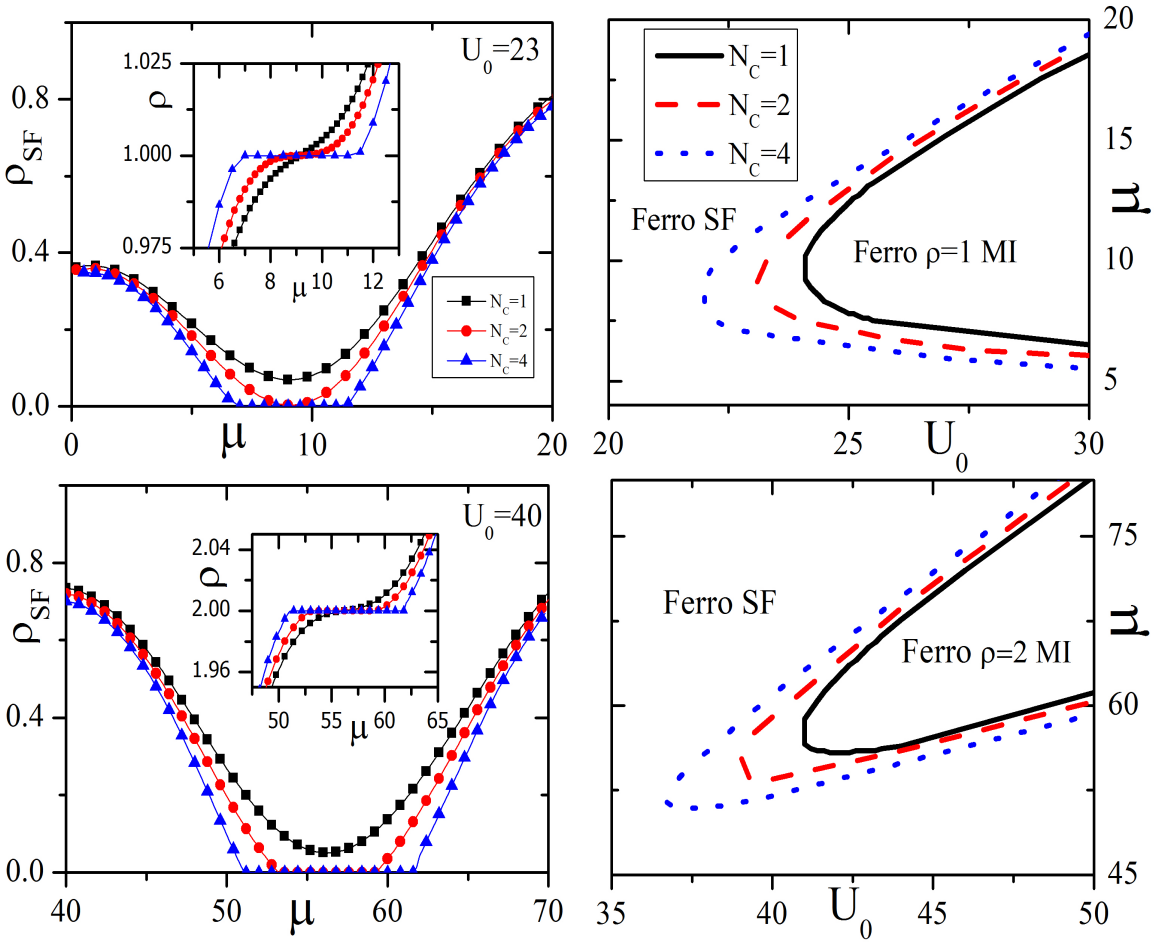


**Figure 8.** Plots of superfluid density $\rho_S$ as function of chemical potential $\mu$ for different values of cluster sizes $N_C$ near density (a)one and (c)two. (inset) Boson density $\rho$ as function of chemical potential $\mu$. Phase diagram obtained for different cluster sizes $N_C$ near density (b)one and (b)two.

and even density Mott insulator is nematic (for low values of interaction $U_2$) or singlet (for large values of interaction $U_2$) and a continuous transition between them. Phase transition between PSF and Nematic MI was known to be a continuous transition from single site mean field theory, is seen to be a weakly first-order transition by using CMFT. For ferromagnetic interaction ($U_2 < 0$), SF and MI phases are Ferromagnetic, and the transition between them is continuous. Critical on-site interaction $U_0^C$ for superfluid to Mott insulator decreases with cluster size. These calculations are numerically less intense than Monte Carlo simulation, but the results are qualitatively same. Recently Rényi Entanglement Entropy has been experimentally measured to characterize SF-MI transitions in case spinless bosons[23]. Calculated Renye's EE shows that Nematic MI is a highly entangled quantum state compared to all other phases of this model. This quantity can be a useful tool to characterize PSF to nematic MI transition for this model. CMFT improves the phase diagram, but we cannot get the information of excitation

spectra in various phases for that we use Random Phase Approximation studies given in the following chapter.

## 2. Cluster Mean Field Theory applied to Spin-1 Bose Hubbard Model:Finite temperatures

In the earlier section using CMFT, we were able to study the magnetic properties in the SF as well as in the MI phases of Spin-1 BH model correctly. In this section, we extend the CMFT formalism to finite temperatures. We describe the formalism below.

The cluster mean-field Hamiltonian is given by (Eq. 4)

$$\begin{aligned}\hat{H}^{cluster} &= -J\sum_{<k,l>,\sigma}^{N_c}(\hat{a}^{\dagger}_{k,\sigma}\hat{a}_{l,\sigma}+H.C)+\frac{U_0}{2}\sum_{k}^{N_c}\hat{n}_k(\hat{n}_k-1)\\ &+\frac{U_2}{2}\sum_{k}^{N_c}(\hat{F}^2_k-2\hat{n_k})-\mu\sum_{k}^{N_c}\hat{n}_k\\ &-t\sum_{k,\sigma}^{N_c}\sum_{l}^{'}(\hat{a}^{\dagger}_{k,\sigma}\psi_{l,\sigma}+\hat{a}_{k,\sigma}\psi^{*}_{l,\sigma}-\psi^{*}_{k,\sigma}\psi_{l,\sigma}).\end{aligned} \tag{7}$$

We construct the cluster Hamiltonian matrix in the Fock's basis of the cluster with an initial guess for $\psi_{k,\sigma}$. Diagonalizing the Hamiltonian matrix we get the eigenvalues $E_\alpha$ and eigenvectors $|\alpha\rangle$. The partition function is given by

$$\mathcal{Z}=\sum_{\alpha}e^{-\frac{E_\alpha}{T}}.$$

The occupation probabilities of each of the cluster mean-field state $|\alpha\rangle$ at any temperature is then equal to

$$P_\alpha=\frac{1}{\mathcal{Z}}e^{-\frac{E_\alpha}{T}}.$$

The thermal averages of any operator is given by

$$\langle\hat{O}\rangle=\sum_{\alpha}P_\alpha\langle\alpha|\hat{O}|\alpha.\rangle.$$

Using these equations, we calculate new SF order parameters $\psi_\sigma=\langle\hat{a_\sigma}\rangle$ and iterate above procedure until the order parameters are obtained self-consistently. This procedure ensures the minimization on Free Energy $\mathcal{F}(\psi_1,\psi_0,\psi_{-1})=-Tln(\mathcal{Z})$. Using the self-consistent eigenstates and eigen values we calculate superfluid density $\rho_{SF}=\sum_\sigma|\psi_\sigma|^2$, and total boson density $\rho=\sum_\sigma\rho_\sigma$ where $\rho_\sigma=\langle\hat{n}_\sigma\rangle$. We also calculate the Nematic order parameter $Q_{zz}=\langle\hat{F}^2_{z,z}-\frac{1}{3}\hat{F}^2\rangle$, singlet density $\rho_{SD}=\langle\hat{A}^{\dagger}_{SD}\hat{A}_{SD}\rangle$ where singlet creation operator $A^{\dagger}_{SD}=\frac{1}{\sqrt{6}}(2a^{\dagger}_1a^{\dagger}_{-1}-a^{\dagger}_0a^{\dagger}_0)$, local magnetic moment $\langle F^2\rangle$, and global magnetic moment $\langle F^2_{TOT}\rangle$ to study the magnetic properties of SF and MI phases. Compressibility $\kappa=\frac{\partial\rho}{\partial\mu}$ is calculated to study transition to NBL. The superfluid and the MI phases undergo a transition to a normal Bose liquid phase(NBL) as temperature is increased. This NBL is characterized by $\rho_{SF}=0$ and $\kappa\neq0$. In this study, we restrict our self for the cluster size $N_C=2$ and present the results below.

*2.1. Anti-Ferromagnetic case*

First, we discuss the anti-ferromagnetic case $U_2 > 0$. The zero temperature phase diagram for $U_2 = 0.03U_0$ has been given in Fig. 5. We choose $U_0 = 24$ to study the finite temperature phase diagram. For this on-site interaction $U_0$, the model (4) has PSF, $\rho = 1$ Nematic MI, and $\rho = 2$ singlet MI phases. Figure 9 shows the evolution of the SF order parameters and the boson densities as a function of temperature in the Polar SF phase at fixed density $\rho = 1.5$. At $T = 0$, we have $\psi_1 = \psi_{-1} \neq 0$ and $\psi_0 = 0$ depicting the polar nature of the SF phase. The existence of small but non-zero $\rho_0$ in the polar superfluid implies that bosons with spin component $\sigma = 0$ are in the NBL state. With the increase in temperature, $\psi_{\pm 1}$ decreases, and vanishes at the SF to NBL transition. The $\psi_0$ however, remain zero. Thus, the polar nature of the SF phase persists even at finite temperatures. It is interesting to note that $\rho_0$ increases on the expense of decrease in $\rho_{\pm 1}$ with increase in the temperature and $\rho_1 = \rho_0 = \rho_-1$ in the NBL phase. The compressibility $\kappa$ shows a maximum at the SF-NBL transition and has no discontinuity seen in the spinless case. Figure 10 shows the comparison of $\rho_{SF}$ calculated from the single site ($N_C = 1$) and two sites cluster ($N_C = 2$) cluster mean-field keeping fixed density $\rho = 1.5$ for various temperature. For all temperatures, we find $\rho_{SF}$ from $N_C = 2$ cluster is lower than single site result. This behavior is expected since CMFT includes some of the quantum fluctuations neglected in the single site mean field calculations. As $T$ increases, the SF density decreases and vanishes in the NBL phase. The critical temperature for SF-NBL transition is lower in the CMFT ($T^C_{N_C=2}$) than the single site mean-field theory ($T^C_{N_C=1}$). This result implies that CMFT has incorporated quantum as well as thermal fluctuations better than the single site mean field theory.

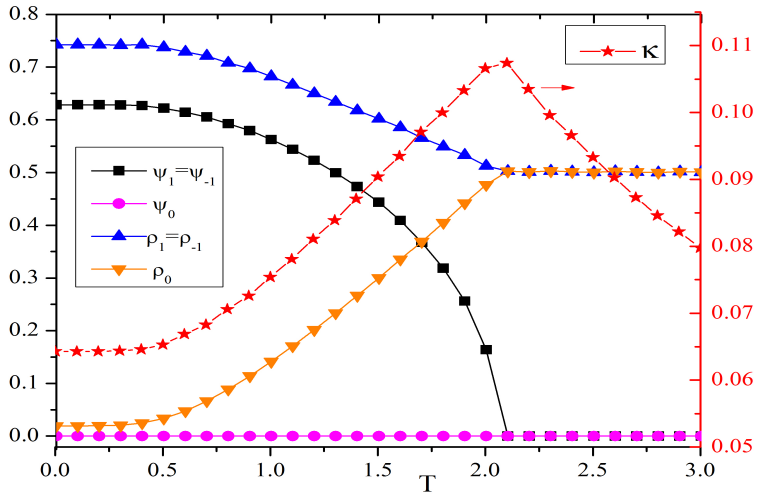


**Figure 9.** Variation of SF order parameters $(\psi_1, \psi_0, \psi_{-1})$, boson densities $\rho_1, \rho_{-1}$ and $\rho_0$, and compressibility $\kappa$ with temperature $T$ for $N_C = 2$ and $\rho = 1.5$. The compressibility $\kappa$ plot has its scale in the right-side axis.

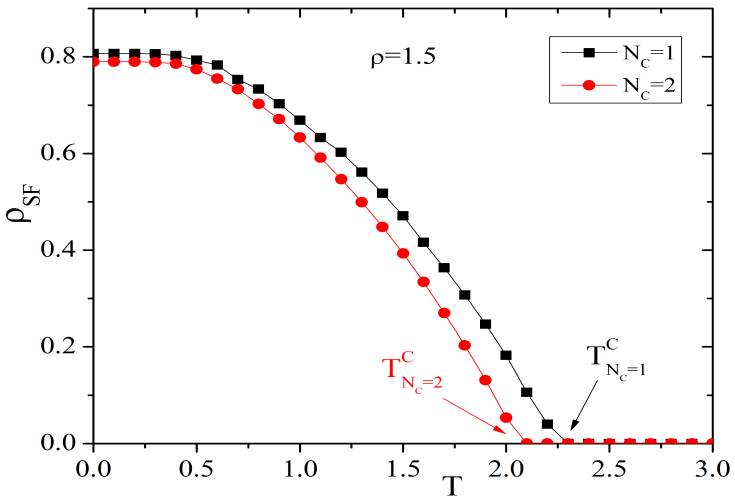


**Figure 10.** Superfluid density $\rho_{SF}$ calculated from the single site ($N_C = 1$) and cluster of $N_C = 2$ sites mean-field theory for different $T$. CMFT predicts lower critical temperature($T^C_{N_C=2}$) for the SF-NBL transition.

We plot, in Figs. 11(a) and (b) respectively for densities $\rho = 1$ and $\rho = 2$, the compressibility $\kappa$ calculated using $N_C = 1$ and $N_C = 2$ mean-field theories for different temperatures to study the transition from MI to NBL. In either case, starting from the MI phases at zero temperature, the compressibility increases with temperature, and the MI phase makes a cross over to NBL. The cluster size is seen to have no prominent effect on this crossover. It is interesting to notice that Nematic ($\rho = 1$) and singlet ($\rho = 2$) MI phase melt to NBL phase at the same rates.

Figure 12 shows the total magnetization of cluster $\langle F^2_{TOT}\rangle$ as a function of $T$ in the $\rho = 1$ MI phase for different ratio of $U_2/U_0$. At zero temperature cluster lowers its energy by minimizing the global magnetization, and this state is predicted to be maximally entangled via quantum fluctuations (Fig. 2). For a small ratio of $U_2/U_0$, small thermal fluctuations are sufficient to break this anti-ferromagnetic arrangement and $\langle F^2_{TOT}\rangle$ increases abruptly. For higher $U_2/U_0$ values; however, the antiferromagnetic coupling is stronger and higher values of temperature are needed to maximize $\langle F^2_{TOT}\rangle$. Other parameters like the magnetic moment of site$\langle F^2\rangle$ and Nematic order parameter $Q_{ZZ}$ do not change significantly inside the $\rho = 1$ Mott insulator.

In the Figs 13(a)-(d) $\langle F^2\rangle$, $\rho_{SD}$, $\langle F^2_{TOT}\rangle$ and $Q_{ZZ}$ are plotted as a function of temperatures for different $U_2/U_0$ ratios in the $\rho = 2$ MI phase. With the increase in thermal fluctuations, the singlet pairs start breaking and $\rho_{SD}$ decreases. This behavior leads to an increase in Nematic order parameter, local and global magnetization.

We now obtain the finite temperature phase diagram of spin-1 Bose Hubbard model. For this purpose we keep $U_0 = 24$ and $U_2 = 0.03U_0$. The superfluid density $\rho_{SF}$, boson density $\rho$ and compressibility $\kappa$ are plotted in Figs. 14(a-d) for temperatures

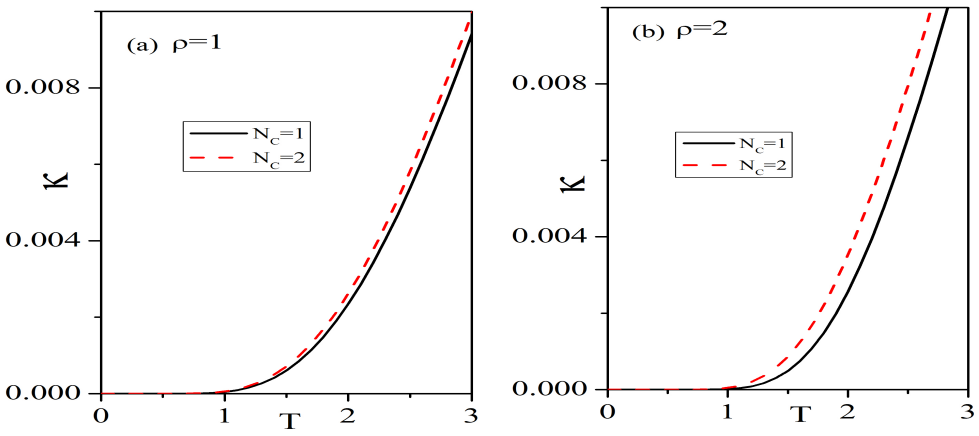


**Figure 11.** Compressibility $\kappa$ is plotted against $T$ starting from (a) $\rho = 1$ MI Nematic phase and (b) $\rho = 2$ singlet phase for cluster sizes $N_C = 1$ and $N_C = 2$. The compressibility calculations are done by keeping densities fixed, i.e $\rho = 1$ and $\rho = 2$ in (a) and (b) respectively.

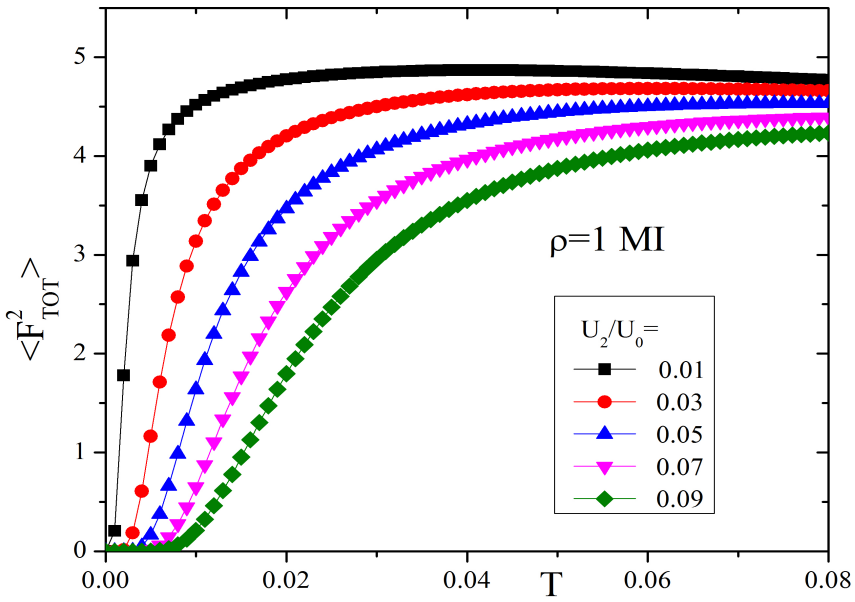


**Figure 12.** Global magnetization of cluster $\langle F^2_{TOT} \rangle$ plotted against $T$ in the $\rho = 1$ MI phase for different $U_2/U_0$ ratios.

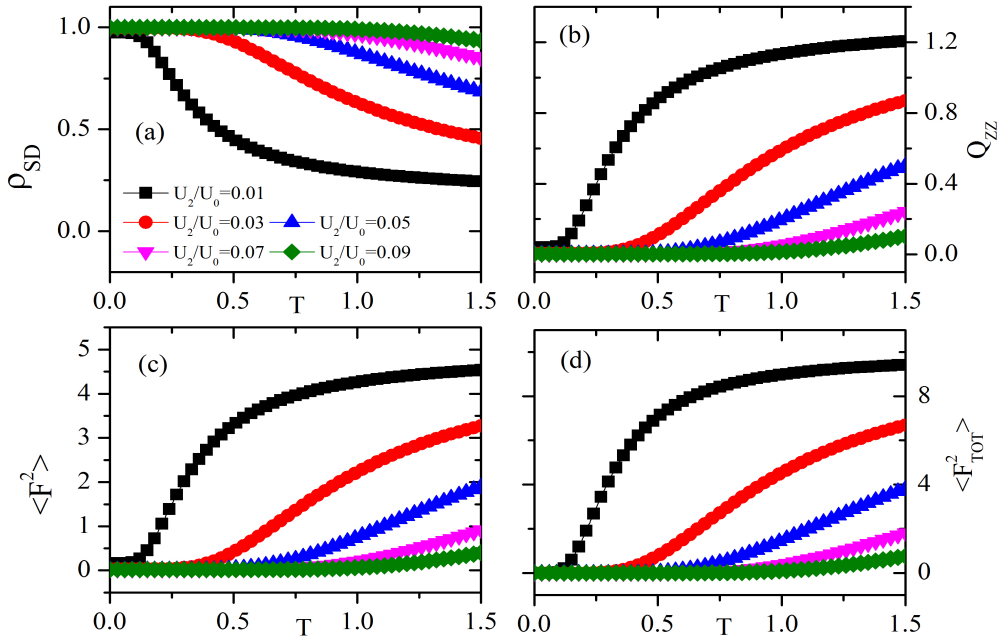


**Figure 13.** Magnetic moment of a site, singlet density, magnetization of cluster and Nematic order as a function of $T$ for different $U_2/U_0$ ratios in $\rho = 2$ MI phase.

$T = 0,\ 0.2,\ 0.8$, and 1.5 respectively. For the same parameters, singlet density $\rho_{SD}$, Nematic order $Q_{ZZ}$, local magnetic moment identifier $\langle F^2 \rangle$, and global magnetic moment identifier $\langle F^2_{TOT} \rangle$ are plotted in Figs. 15(a-d). We observe the following. At $T = 0$, the compressibility $\kappa$ is non-zero in polar SF phase but zero in MI phases. It has a jump at the SF-MI phase transition. For small temperatures, for example, $T = 0.2$, $\kappa$ is very small in the MI phases compared to that in polar SF phase. However, the Mott region with a density of $\rho = 1$ is enlarged. The thermal fluctuations break the highly entangled Anti-Ferro magnetic arrangement of the spins in the cluster in the $\rho = 1$ MI, whereas no such changes are seen in the SF and $\rho = 2$ singlet MI phases at this temperature. Also, $\kappa$ shows a notable jump at polar SF to $\rho = 1$ MI transition. For higher temperatures, say $T = 0.5$ the SF density in polar SF phase is reduced, and an NBL phase is seen to emerge between the polar SF and $\rho = 1$ MI phases. The thermal fluctuations present here reduces the singlet density slightly in the $\rho = 2$ MI and increases the local and magnetic moment. With further increase in temperature to $T = 1.5$, SF density is seen to reduce further, and the NBL phase emerges at the boundaries of polar SF and MI transition. The singlet pairing in $\rho = 2$ MI is greatly reduced due to the thermal fluctuations.

We plot the phase diagram in the $\mu$-$T$ plane for $U_0 = 24$ and $U_2 = 0.03\ U_0$ in Fig. 16. The MI to NBL transition is a crossover and to mark the MI phase, we have considered two cases: (i) the points where $\rho_{SF} = 0$ and $\kappa < 0.0001$ and (ii) the points where

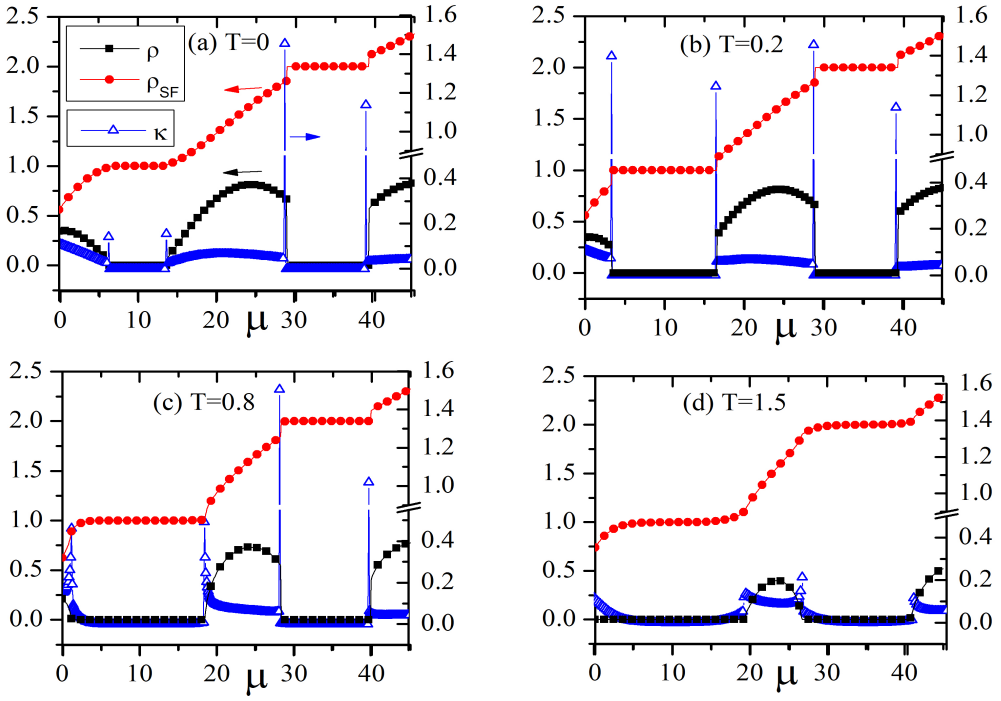


**Figure 14.** The superfluid density $\rho_{SF}$, boson density $\rho$, and compressibility $\kappa$ plotted against chemical potential $\mu$ for cluster size $N_C = 2$ at temperatures (a) $T = 0$, (b) $T = 0.2$, (c) $T = 0.8$, and (d) $T = 1.5$. We keep $U_0 = 24$ and $U_2/U_0 = 0.03$. Direction of arrows indicate scale to follow.

$\rho_{SF} = 0$ and $\kappa < 0.03$. We observe that $\rho = 1$ Mott phase enlarges with temperature due to the breaking of the antiferromagnetic alignment of the spins in the cluster. No such effect is seen in the $\rho = 2$ MI phase because of the singlet formation. There is a transition from PSF-MI-NBL with temperature when the density is close to unity. It is interesting to notice that even though small thermal fluctuations are sufficient to break the ground state of highly entangled $\rho = 1$ Nematic MI compared to thermally robust $\rho = 2$ singlet MI, both Mott phases melt to NBL phase at the same temperature.

### *2.2. Ferromagnetic case*

We now move to the ferromagnetic case. The zero temperature phase diagrams (Figs. 8(b) and (d)) show SF, and MI phases are ferromagnetic, and the transition between them is always continuous. The finite temperature results from CMFT with $N_C = 2$ are given below, for a typical $U_0 = 42$ and $U_2/U_0 = -0.03$.

The plot transition from the SF to NBL phase in Fig. 17(a). As the temperature increases, $\psi_1 = \psi_{-1}$ and $\psi_0$ starts decreasing and vanishes in the NBL phase. The ferromagnetic nature of the SF, $\psi_1 = \psi_{-1}$ and $\psi_0 = \sqrt{2}\psi_1$, is satisfied for all temperatures. $\rho_1 = \rho_{-1}$ increases at the expense of a decrease in $\rho_0$ until all three densities become equal in the NBL phase. Compressibility $\kappa$ shows a maximum at the

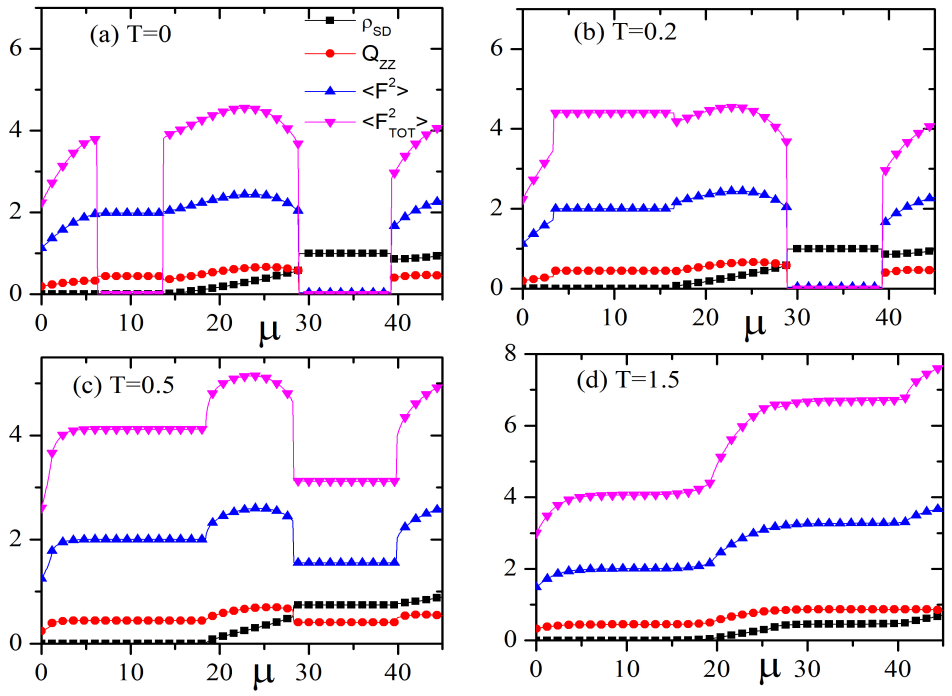


**Figure 15.** The singlet pair density $\rho_{SD}$, Nematic order parameter $Q_{ZZ}$, local magnetic moment identifier $\langle F^2 \rangle$, and $\langle F^2_{TOT} \rangle$ plotted against chemical potential $\mu$ for cluster size $N_C = 2$ at temperatures (a) $T = 0$, (b) $T = 0.2$, (c) $T = 0.8$, and (d) $T = 1.5$ keeping $U_0 = 24$ and $U_2/U_0 = 0.03$.

Ferro SF to NBL phase transition. Further, in the Fig. 17(b) we compare the SF-NBL transition with cluster sizes $N_C = 1$ and $N_C = 2$ keeping density fixed. We find $\rho_{SF}$ obtained from CMFT is smaller than that from the single site MFT. We expect this behavior since CMFT includes quantum fluctuations neglected by the single site MFT. The CMFT predicts lower $T_C$ (critical temperature for the SF-NBL transition) compared to the single site mean field theory.

Figure. 18 shows comparison of compressibility $\kappa$ starting from zero temperature $\rho = 1$ and $\rho = 2$ MI lobes for various temperatures. Increase in $\kappa$ with temperature signifies melting of the MI phase to the NBL phase. We find the MI-NBL transition temperature is independent of the density of the Mott lobe.

The finite temperature effect on the magnetic properties inside $\rho = 1$ MI phase is studied in Fig. 19. The local magnetic moment $\langle F^2 \rangle$ does not change much with the increase in temperature whereas the global magnetization $\langle F^2_{TOT} \rangle$ is seen to reduce and saturate at high temperatures for all values of $U_2/U_0$.

In Fig. 20 we plot the superfluid density $\rho_{SF}$, the boson density $\rho$, and the compressibility $\kappa$ for different chemical potentials $\mu$ for temperatures $T = 0, 0.2, 1$ and 1.5. We also plot, for the same parameters, the local magnetic moment and global magnetic moment in Fig. 21. The $\kappa = 0$ with $\rho_{SF} = 0$ represents $\rho = 1$, 2 MI

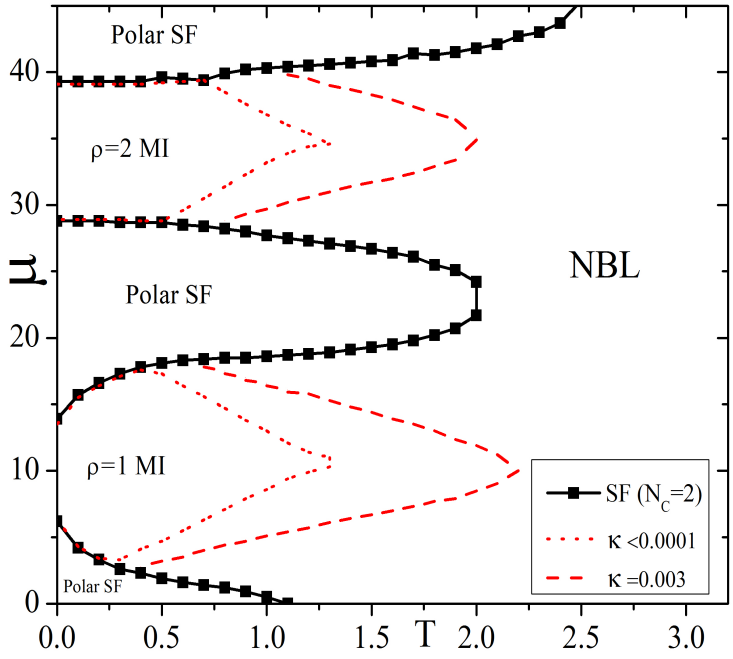


**Figure 16.** $\mu - T$ phase diagram for $U_0 = 24$ and $U_2/U_0 = 0.03$

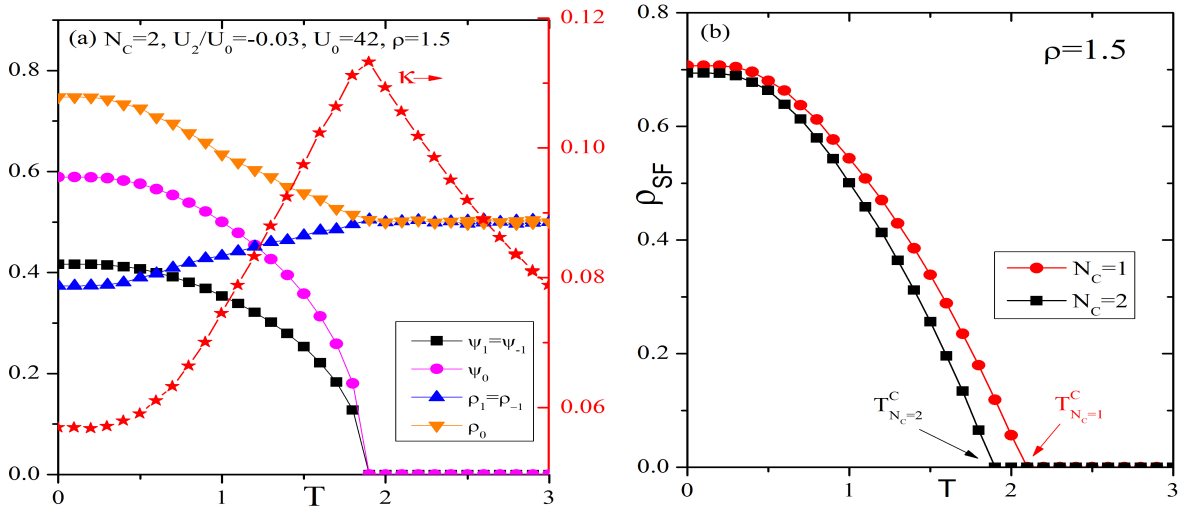


**Figure 17.** (a) Variation of SF order parameters $(\psi_1, \psi_0, \psi_{-1})$ and boson densities $(\rho_1, \rho_{-1}, \rho_0)$ with temperature $T$ for $\rho = 1.5$. Compressibility $\kappa$ is also plotted with its scale given in the right-side axis. (b) The SF density $\rho_{SF}$ calculated from single site $(N_C = 1)$ and cluster of $N_C = 2$ sites MFT against $T$.

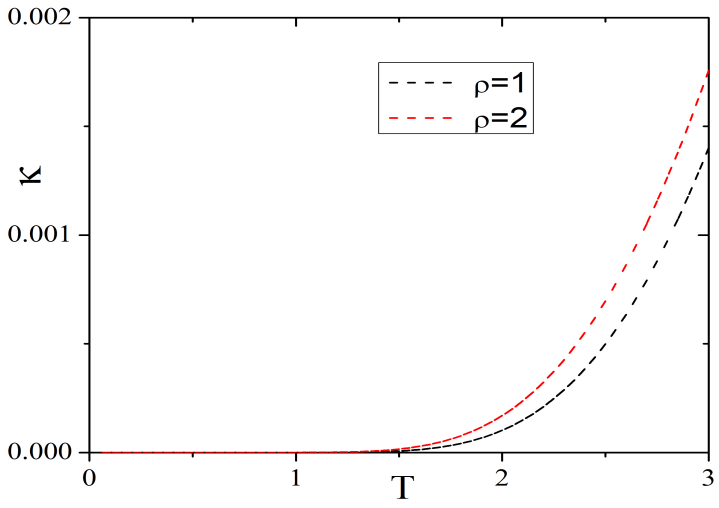


**Figure 18.** Compressibility $\kappa$ is plotted against $T$ for $\rho = 1$ and $\rho = 2$ Ferro MI phases.

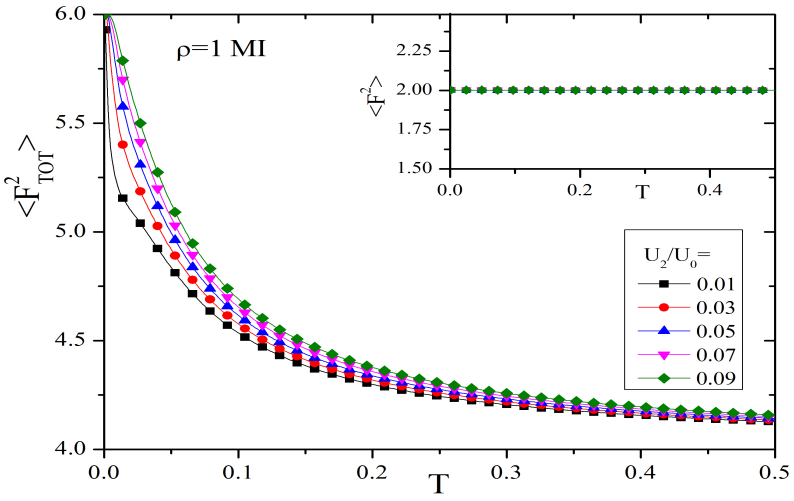


**Figure 19.** Global magnetization of the cluster $\langle F^2_{TOT} \rangle$ plotted against $T$ for $\rho = 1$ MI phase for different $U_2/U_0$ ratios. (inset) Local magnetic moment identifier $\langle F^2 \rangle$ against $T$ in $\rho = 1$ MI phase.

phases. The SF-MI transition is continuous in the zero temperature. As we increase the temperature, say $T = 0.2$, Fig. 20(b) shows that SF-MI transition becomes discontinues. The local magnetic moment remains maximized in MI phases, but we find a reduction in the global magnetic moment. Also, MI phases have enlarged. When the temperature is increased further to $T = 1$ and $T = 1.5$, SF density reduces, and an envelope of NBL phase form around the MI phases. Also, the global magnetization reduces with increase in temperature.

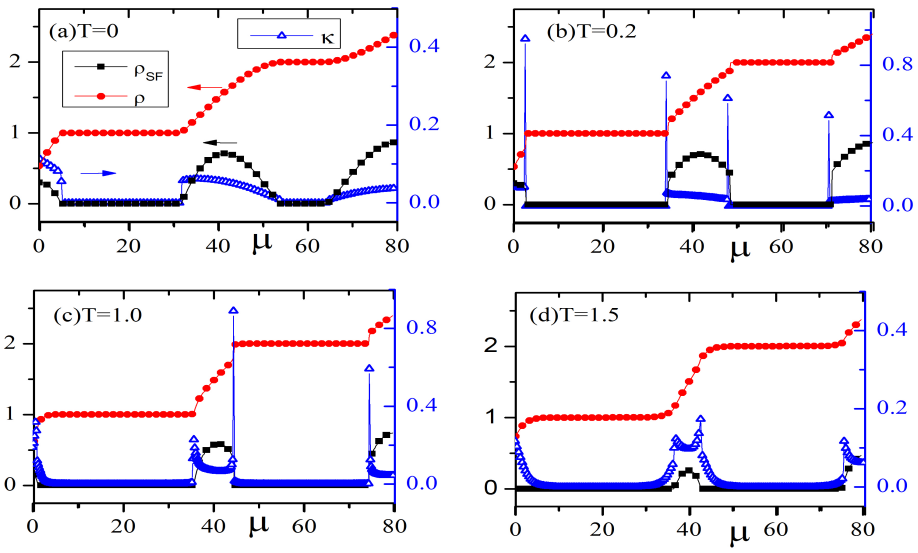


**Figure 20.** Plots of the superfluid density$\rho_{SF}$, boson density $\rho$ and the compressibility $\kappa$ versus chemical potential $\mu$ at temperatures (a) $T = 0$, (b) $T = 0.2$, (c) $T = 1$ and (d) $T = 1.5$. $U_0 = 42$ and $U_2/U_0 = -0.03$. Direction of arrows indicate scale to follow.

We plot the phase diagram in $\mu - T$ plane in Fig. 22. Phase boundary for MI-NBL transition is selected for $\kappa \leq 0.0001$ and $\kappa < 0.005$ to mark the MI-NBL crossover. We also observe $\rho = 1$ and $\rho = 2$ MI phases melt to NBL phase at the same rate.

### *2.3. Conclusion*

The finite temperature RPA and Cluster Mean Field formalism are developed here. Using these methods finite temperature properties of soft-core and spin-1 Bose Hubbard model are studied in detail. Using RPA equations the speed of sound and the momentum distribution are calculated for SC-BH modeland it shows interesting results. The sound velocity is seen to decrease smoothly as with increase in thermal fluctuations and becomes zero in NBL phase. Also the peak in momentum distribution in SF phase is seen to diminish as one goes into NBL phase by increasing the temperature. This gives the experimental signature of SF o NBL transition.

For Spin-1 BHM at nonzero temperatures, Polar or Ferro nature of SF persists and PSF-Nematic MI transition becomes strongly first order. Even though very low

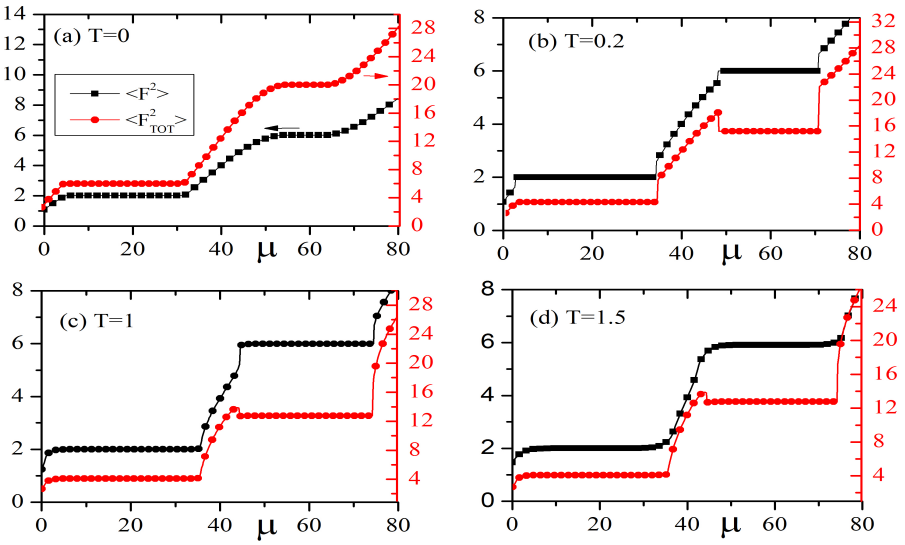


**Figure 21.** Plots of local magnetic moment identifier $\langle F^2 \rangle$ and $\langle F^2_{TOT} \rangle$ versus the chemical potential $\mu$ at temperatures (a) $T = 0$, (b) $T = 0.2$, (c) $T = 1$ and (d) $T = 1.5$. $U_0 = 42$ and $U_2/U_0 = -0.03$. Direction of arrows indicate scale to follow.

thermal fluctuations are sufficient to destroy the density one Nematic phase compared to the robust singlet MI, both MI phases melt to NBL phase at same rates. The MI-NBL transition is like a crossover and the transition temperature cannot be identified. Altogether, the MI to NBL transition do not prominently depend on the density or its magnetic structure. The major affect of the magnetic interactions are reflected while studying SF to MI transitions at zero and finite temperatures.

## 3. Phase Transitions of Spin-1 Bosons in an Optical Superlattice

### *3.1. Introduction*

Ultracold atoms in optical lattices and superlattices provide us with the realization of engineered quantum many-body lattice models [24, 25, 26]. One remarkable development in this context is the realization of Bose gases in the optical lattices. Superfluid (SF) to Mott Insulator (MI) quantum phase transition in cold bosonic atoms has received great scientific attention since its theoretical prediction in the context of Bose Hubbard model (BHM) and followed by its experimental realization [27]. When traps are purely optical, Alkali atoms like $^{87}Rb$, $^{23}Na$ and $^{30}K$, with hyperfine spin F=1, have spin degrees of freedom, and thus, the interaction between bosons is spin-dependent [1, 2]. The interaction is ferromagnetic (e.g. $^{87}Rb$) or anti-ferromagnetic (e.g. $^{23}Na$), depending upon scattering lengths of singlet and quintuplet channels [1]. The spin-dependent interaction in spinor gases exhibits richer quantum effects than their single-component counterparts, and it not only modifies the nature of phase diagrams but also allows the study of superfluidity and magnetism.

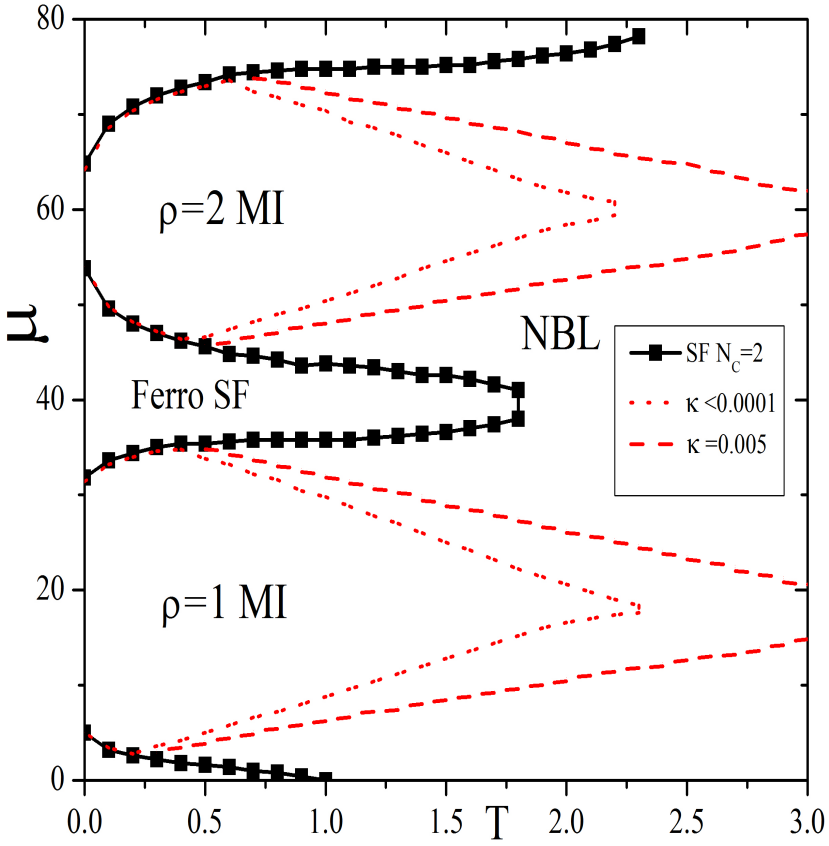


**Figure 22.** $\mu - T$ phase diagram for $U_0 = 42$ and $U_2/U_0 = -0.03$

The optical superlattices are obtained by the superimposition of two monochromatic lattices with slightly different wavelengths [28]. When the relative phase between the two standing waves and their respective depths vary independently, a periodic pattern of potential wells with two different depths at two adjacent sites is obtained. This difference in the depth of two nearby sites is the measure of superlattice potential. In this report, we investigate spin-1 ultracold bosons loaded into 2-dimensional bi-chromatic optical superlattices.

*3.2. Methodology*

The spin-1 BoseHubbard model, which describes spin full bosons in an optical superlattice, is given by;

$$\mathcal{H} = -t \sum_{<i,j>,\sigma} (a^{\dagger}_{i,\sigma} a_{j,\sigma} + a^{\dagger}_{j,\sigma} a_{i,\sigma}) + \frac{U_0}{2} \sum_i \hat{n}_i(\hat{n}_i - 1) + \frac{U_2}{2} \sum_i (\overrightarrow{F}_i^2 - 2\hat{n}_i) - \sum_i \mu_i \hat{n}_i \tag{8}$$

where first term represents hopping of bosons between nearest neighbour sites $< i, j >$ with an amplitude $t$. Here $a_{i,\sigma}(a^{\dagger}_{i,\sigma})$ represents annihilation (creation) operator at site $i$ with spin projection $\sigma = \{-1, 0, 1\}$, number operator $\hat{n}_{i,\sigma} = a^{\dagger}_{i,\sigma} a_{i,\sigma}$ and $\hat{n}_i = \sum_{\sigma} \hat{n}_{i,\sigma}$. Spin operator $\overrightarrow{F}_i = (F_i^x, F_i^y, F_i^z)$ where $F_i^{\alpha} = \sum_{\sigma,\sigma'} a^{\dagger}_{i,\sigma} S^{\alpha}_{\sigma,\sigma'} a_{i,\sigma'}$ with $\alpha = x, y, z$ and $S^{\alpha}_{\sigma,\sigma'}$ are standard spin-1 matrices. Spin independent (dependent) interaction $U_0(U_2)$ arises due to the difference in the scattering length $a_0$ and $a_2$ in the spin S=0 and S=2 channels respectively. The spin dependent interaction $U_2$ can be positive (anti-ferromagnetic) or negative (ferromagnetic) depending on the values of $a_0$ and $a_2$[1]. The site dependent chemical potential $\mu_i = \mu + (-1)^i \delta$ where $\mu$ controls the bosons density and $\delta$ is the shift in energy due to superlattice potential. Here, we consider a bi-chromatic superlattice and thus, the whole lattice is bipartite into A and B sub-lattices with $\mu_A = \mu + \delta$ and $\mu_B = \mu - \delta$.

In the cluster mean-field theory [21, 29], the entire lattice is divided into clusters with $N_C$ number of sites. In this calculation, we take $N_C = 2$ and thus, each cluster consists of one site each from A and B sub-lattices. We first decouple each cluster from its nearest neighbor clusters using standard mean-field procedure [**?**]. The resultant the model 9 is given by

$$\mathcal{H} = \sum_{clusters} \mathcal{H}^C \tag{9}$$

$$\begin{aligned} \mathcal{H}^C = & -t \sum_{\sigma} (a^{\dagger}_{A,\sigma} a_{B,\sigma} + a^{\dagger}_{B,\sigma} a_{A,\sigma}) \\ & - 3t \sum_{\sigma} [(a_{A,\sigma} + a_{A,\sigma}) \psi_{B,\sigma} + (a_{B,\sigma} + a_{B,\sigma}) \psi_{A,\sigma} - 2\psi_{A,\sigma} \psi_{B,\sigma}] \\ & + \frac{U_0}{2} \sum_{i=A,B} \hat{n}_i(\hat{n}_i - 1) + \frac{U_2}{2} \sum_{i=A,B} (\overrightarrow{F}_i^2 - 2\hat{n}_i) \\ & - \sum_{\sigma} (\mu_A \hat{n}_{A,\sigma} + \mu_B \hat{n}_{B,\sigma}) \end{aligned} \tag{10}$$

Here $\psi_{A,\sigma} = \langle a_{A,\sigma} \rangle (\psi_{B,\sigma} = \langle a_{B,\sigma} \rangle)$ is the A(B) sub-lattice superfluid order parameter with spin component $\sigma$. We determine $\psi_{A,\sigma}$ and $\psi_{B,\sigma}$ self-consistently using the method described in Ref. [29]. Sub-lattice superfluid densities $\rho^S_{A(B)} =$

$\sum_{\sigma} \left|\psi_{A(B),\sigma}\right|^2$ and densities of bosons $\rho_{A(B)} = \langle \hat{n}_{A(B)} \rangle$ are calculated from this self-consistently determined ground state. We also calculate the average density of bosons $\varrho = \frac{1}{2}(\rho_A + \rho_B)$ and the density wave order parameter $O_{DW} = |\rho_A - \rho_B|$ . We can characterize the ground state of model 9 from these quantities. The ground state is a superfluid (Mott insulator) if $\rho^S_{A(B)}$ is non-zero (zero). The magnetic properties of the superfluid and Mott insulator phases are determined from Nematic order parameter $Q^{\alpha,\alpha}_{A(B)} = \left\langle F^{\alpha}_{A(B)} F^{\alpha}_{A(B)} - \frac{1}{3}\langle F^2_{A(B)} \rangle \right\rangle$ and singlet pair density $\rho^{SD}_{A(B)} = \langle \hat{A}^{\dagger}_{A(B)} \hat{A}_{A(B)} \rangle$, where the singlet creation operator $\hat{A}^{\dagger}_{A(B)} = \left( 2a^{\dagger}_{A(B),1} a^{\dagger}_{A(B),-1} - a^{\dagger}_{A(B),0} a^{\dagger}_{A(B),0} \right)$ . In addition to these quantities, we also investigate entanglement properties [11] of different ground states by calculating Rényi entanglement entropy (EE) given by $S_2[A(B)] = -log[Tr(\rho^2_{A(B)})]$ where $\rho_{A(B)}$ is the reduced density matrix for sub-lattice A (B)[12].

### *3.3. Results: Antiferromagnetic Case*

We now present the results of the Cluster Mean Field Theory applied to 2-dimensional spin-1 Bose Hubbard model in bi-chromatic superlattice, with cluster size $N_C = 2$. Here we restrict ourselves to the anti-ferromagnetic case $U_2 > 0$. We set our energy scale by choosing $t = 1$ and thus all parameters are dimensionless. It is known from the earlier studies that, for the anti-ferromagnetic case ( $U_2 > 0$), the symmetry the superfluid phase is polar (PSF) and in the mean-field level symmetry restricts values of the superfluid order parameters such that either $\psi_{A(B),1} = \psi_{A(B),-1} \neq 0$, $\psi_{A(B),0} = 0$ or $\psi_{A(B),1} = \psi_{A(B),-1} = 0$ and $\psi_{A(B),0} \neq 0$[29]. Superfluid order parameters are plotted in the 23(a) for $U_0 = 30$, $U_2 = 0.03U_0$ and superlattice potential $\delta = 6$. It is evident from the 23(a) that the superfluid phases have polar symmetry: we find $\psi_{A(B),1} = \psi_{A(B),-1} \neq 0$ and $\psi_{A(B),0} = 0$ and thus, superlattice potential do not change this symmetry. There are four regions in the chemical potentials where $\psi_{A(B),\sigma} = 0$ thus, correspond to four insulator phases. The sublattice bosons densities $\rho_A$ and $\rho_B$, the average boson density $\varrho = \frac{1}{2}(\rho_A + \rho_B)$ and the density wave order parameter $O_{DW}$ are plotted in the 23(b).

The four insulator regions have average densities $\rho = \frac{1}{2}, 1, \frac{3}{2}$ and 2 with sublattice densities $(\rho_A, \rho_B) = (1,0), (1,1), (2,1)$ and $(2,2)$ respectively. Insulators with the density $\rho = 1$ and 2 are the normal Mott insulators where the density is uniform across whole lattice and $O_{DW} = 0$. However, insulators with $\rho = \frac{1}{2}$ and $\frac{3}{2}$ have finite $O_{DW}$ and are called density wave insulators. Thus, the superlattice potential introduces additional insulator phases with half-integer bosons densities. The sublattice bosons densities with different spin component $\rho_{A(B),\sigma}$ are plotted in the 23(c). In general, we find $\rho_{A(B),\pm 1} > \rho_{A(B),0}$ except in the Mott insulator region, i.e., for $\rho = 1$ and 2, we find $\rho_{A,\pm 1} = \rho_{A,0} = \rho_{B,\pm 1} = \rho_{B,0}$. It should be noted here that the symmetry of the polar superfluid phase is such that $\psi_{A(B),1} = \psi_{A(B),-1} \neq 0$, $\psi_{A(B),0} = 0$. This imply that the bosons with spin component $\sigma = 0$, though present in the system are not in the superfluid phase. Only bosons with spin component $\sigma = \pm 1$ form superfluid. This

leads to a situation where we have a two-fluid model with bosons with $\sigma = \pm 1$ are in superfluid phase while bosons with $\sigma = 0$ are in the normal fluid phase. Magnetic properties of the superfluid and the insulating phases are given in the 23(d) where we plot Nematic order parameter $Q^{z,z}_{A(B)}$ and singlet pair density $\rho^{SD}_{A(B)}$. We find that density $\rho = 2$ Mott insulator phase is a singlet phase with $\rho^{SD}_A = \rho^{SD}_B = 1$ and $Q^{z,z}_A = Q^{z,z}_B = 0$.

The density $\rho = 1$ Mott insulator phase, however, is nematic $Q^{z,z}_A = Q^{z,z}_B > 0$ and $\rho^{SD}_A = \rho^{SD}_B = 0$. In $\rho = \frac{1}{2}$ density wave insulator, the sublattice boson densities are $(\rho_A, \rho_B) = (1, 0)$. In this phase we find $Q^{z,z}_A > 0, Q^{z,z}_B = 0$ and $\rho^{SD}_A = \rho^{SD}_B = 0$ . In the $\rho = \frac{3}{2}$ density wave insulator, however, $Q^{z,z}_B > 0, Q^{z,z}_A = 0$ and $\rho^{SD}_A = 1, \rho^{SD}_B = 0$. So, in the $\rho = \frac{3}{2}$ density wave insulator, A-sublattice is in the singlet phase and B-sublattice is in the nematic phase, whereas in the$\rho = \frac{1}{2}$ density wave insulator, A-sublattice is in the nematic phase. We present the results for Rényi EE in 24. In general, we find $S_2[A] = S_2[B]$ and are very small except in the $\rho = 1$ Mott insulator where $S_2$ is two orders of magnitude larger. $S_2$ is constant in insulating phases and vary with chemical potential in polar superfluid phases.

We plot the phase diagram of model 10 for $\delta$= 6 and 10 in 25(a) and (b) respectively. There are four insulating phases represented by lobes. The dotted lines represent phase diagram for $\delta$= 0 where there are only two lobes correspond to $\rho$ =1 and 2 Mott insulator phases. As we introduce the superlattice potential, these two Mott phases shrink and two additional density wave insulating phases form with average density $\rho = \frac{1}{2}$ and $\frac{3}{2}$. We also observed that these density wave insulator lobes enlarge with superlattice potential.

### *3.4. Conclusion*

In our present work, we use the cluster mean field theory to study the behavior of spin-1 bosons in the optical superlattices. Since intra-site fluctuations are treated exactly in CMFT, it permits us to study the magnetic and the superfluid properties of the system simultaneously. Our investigation primarily focused on the anti ferromagnetic case ($U_2 > 0$). We conclude that, in bi-chromatic superlattices, the introduction of superlattice potential favours the localisation of the bosons and this leads to density wave Mott insulators. When $\delta$=0, we have uniform superfluid and Mott insulator phases. As $\delta$ increases, the uniform Mott insulator lobes shrink while the half integer density wave insulator lobes enlarge. The symmetry of the superfluid phase remains unaffected by the superlattice potential. We have also studied the magnetic properties of insulating phases as well as calculated Rényi EE. We found that the $\rho$ ==1 Mott lobe is nematic, and $\rho$ ==2 lobe a singlet. The magnetic property of the density wave insulator, however, depends on the sub-lattice density. Rényi EE remains mostly small except at density $\rho$ ==1 Mott insulator and could be used as a marker of the transition.

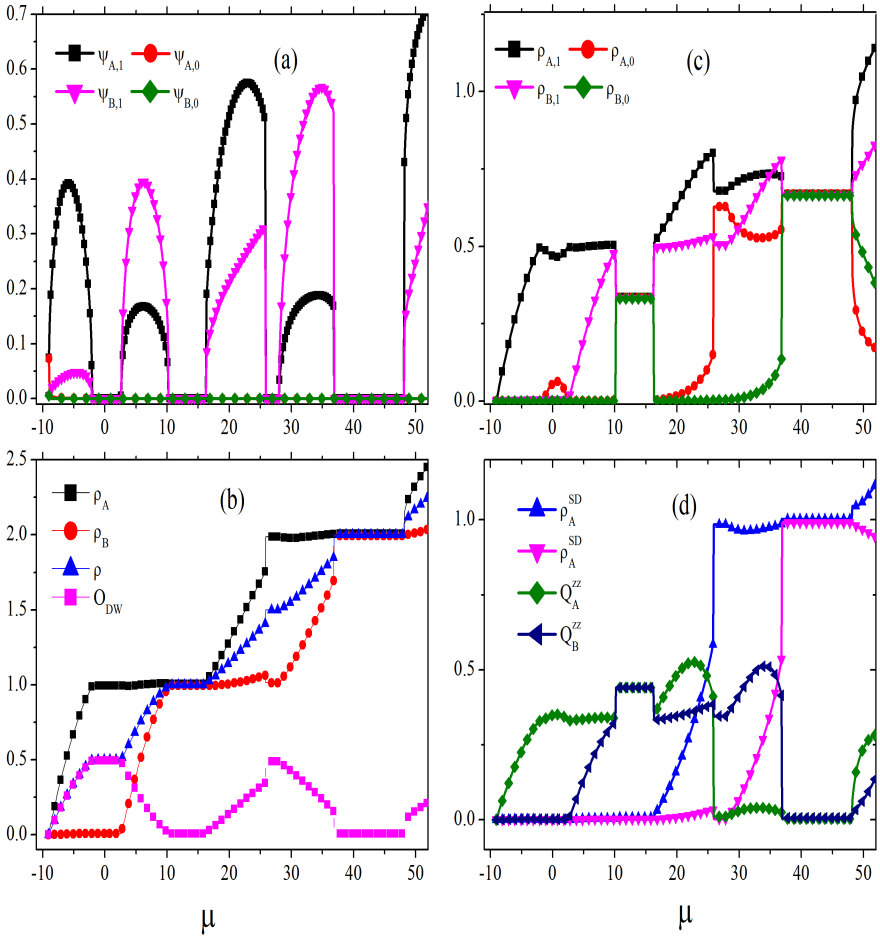


**Figure 23.** (Colour online) (a) Superfluid order parameters, (b) densities and density wave order parameters, (c) densities with spin component $\sigma$ and (d) nematic order and singlet pair density are plotted as a function of chemical potential $\mu$ for $U_0 = 39$, $U_2 = 0.03U_0$ and $\delta = 6$.

### *3.5. Results: Ferromagnetic Case*

We now present the results of the Cluster Mean Field Theory applied to 2-dimensional spin-1 Bose Hubbard model in bi-chromatic superlattice, with cluster size $N_C = 2$. Here we restrict ourselves to the ferromagnetic case $U_2 < 0$. We set our energy scale by choosing $t = 1$ and thus all parameters are dimensionless. It is known from the earlier studies that, for the anti-ferromagnetic case ( $U_2 > 0$), the symmetry the superfluid phase is polar (PSF) and for ferromagnetic case ($U_2 < 0$) it is a ferromagnetic superfluid phase (FSF)[29]. In the mean-field level, A ferromagnetic superfluid is characterized by $\psi_{A(B),1} = \psi_{A(B),-1} \neq \psi_{A(B),0}$ and a relation between superfluid order parameters is such that $\psi_{A(B),0} = \sqrt{2}\psi_{A(B),\pm1}$. Superfluid order parameters are plotted in the 26(a) for $U_0 = 39$, $U_2 = -0.03U_0$ and superlattice potential $\delta = 6$. It is evident from the 26(a)

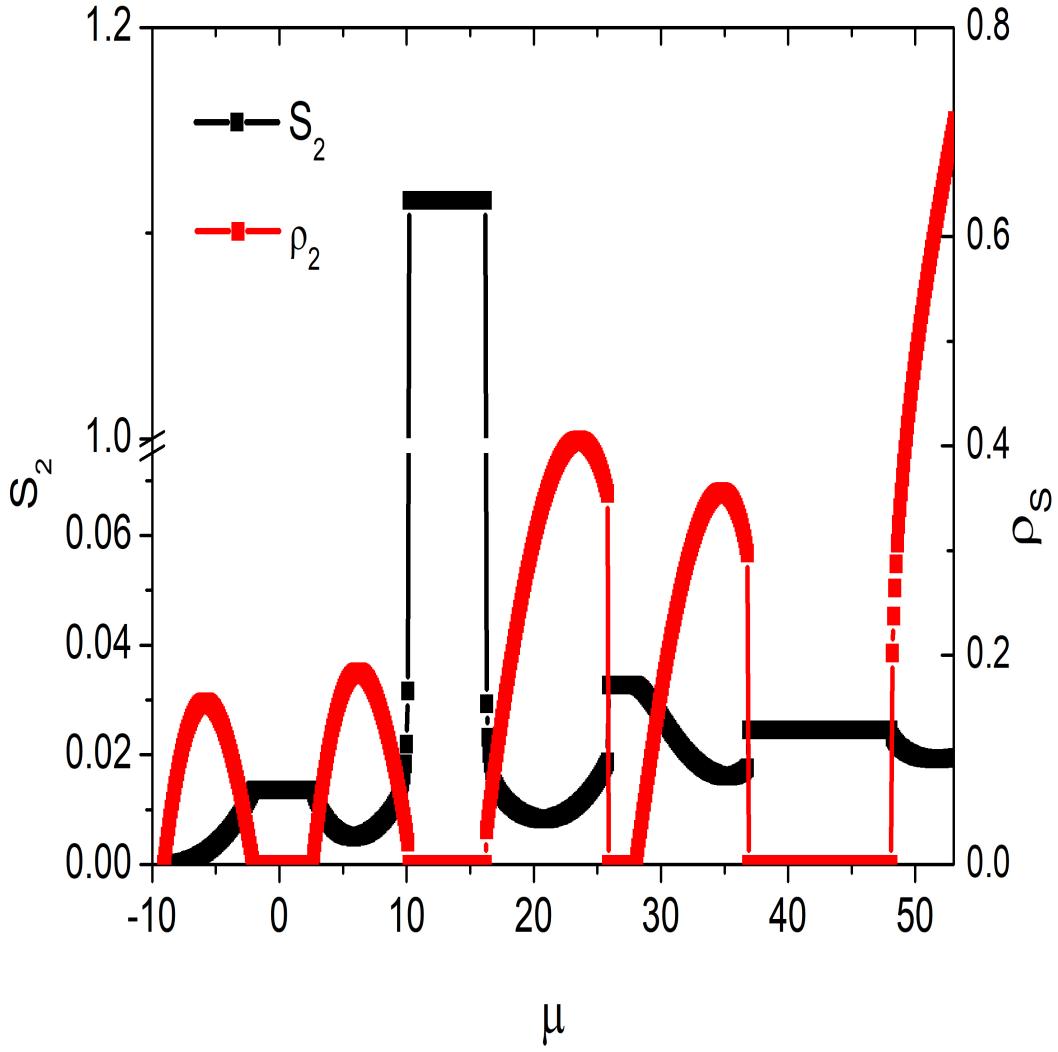


**Figure 24.** (Colour online) RényiEE $S_2$ and superfluid density $\rho_S$ are plotted as a function of chemical potential $\mu$ for $U_0 = 30$, $U_2 = 0.03U_0$ and $\delta = 6$.

that the superfluid phases have ferromagnetic symmetry: we find $\psi_{A(B),0} = \sqrt{2}\psi_{A(B),\pm 1}$ and thus, superlattice potential do not change this symmetry. There are two regions in the chemical potentials where $\psi_{A(B),\sigma} = 0$ thus, correspond to two insulator phases. Since we are looking at a ferromagnetic system, Mott insulator phase with density $\rho$= 2 appears at higher interaction potential as can be seen from 28(a). The sublattice bosons densities $\rho_A$ and $\rho_B$, the average boson density $\varrho = \frac{1}{2}(\rho_A + \rho_B)$ and the density wave order parameter $O_{DW}$ are plotted in the 26(b).

The insulator regions have average densities $\rho = \frac{1}{2}, 1, \frac{3}{2}\&2$ with sublattice densities $(\rho_A, \rho_B) = (1,0), (1,1), (2,1)\&(2,2)$ respectively. Insulators with the density $\rho = 1$ is the normal Mott insulators where the density is uniform across whole lattice and $O_{DW} = 0$. However, insulators with $\rho = \frac{1}{2}$ and $\frac{3}{2}$ have finite $O_{DW}$ and are called density wave insulators. Thus, the superlattice potential introduces additional insulator phases

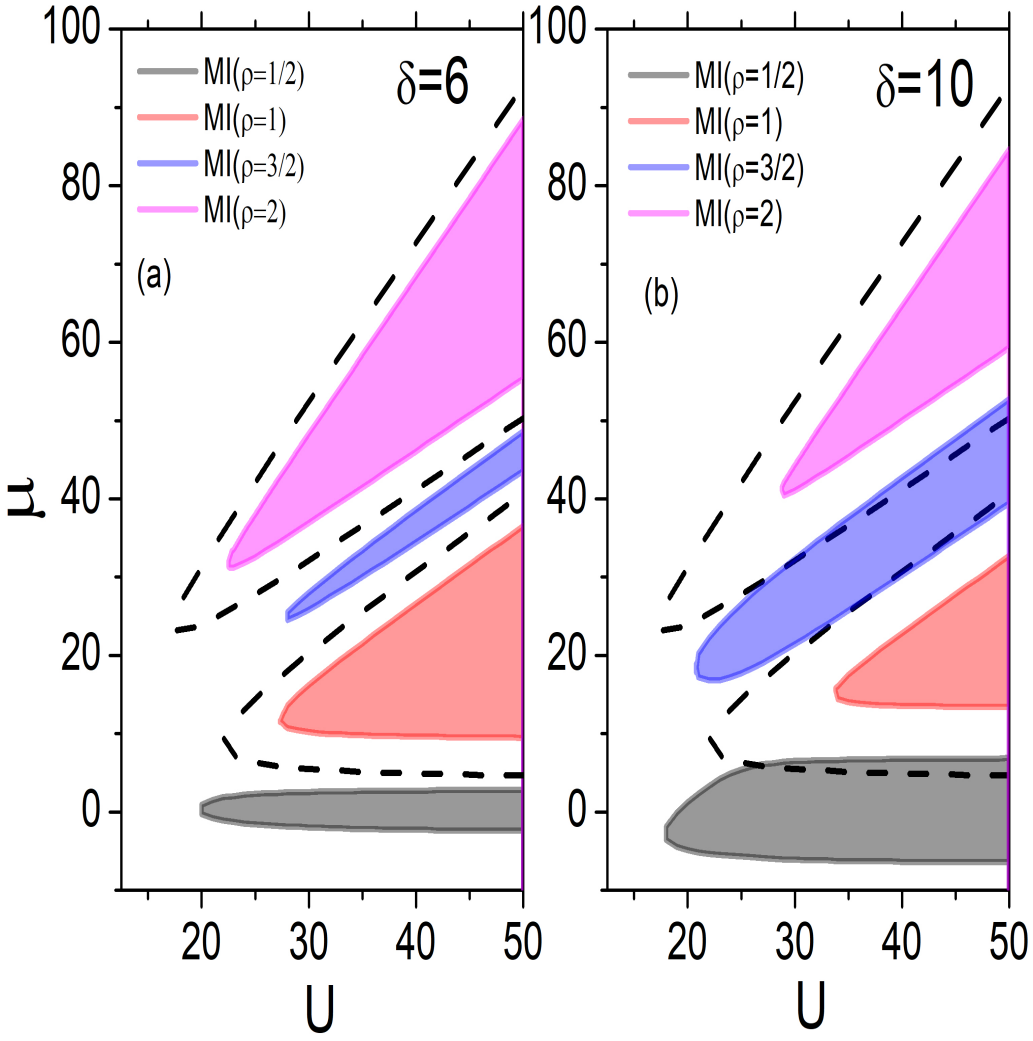


**Figure 25.** (Colour online) Phase diagram of model (1) for (a)$\delta = 6$ and (b) $\delta = 10$. The coloured lobes are insulating phases and rest of the region is polar superfluid. The dashed line represent the phase diagram for $\delta = 0$.

with half-integer bosons densities. The sublattice bosons densities with different spin component $\rho_{A(B),\sigma}$ are plotted in the 26(c). In general, we find $\rho_{A(B),0} > \rho_{A(B),\pm1}$ and follows the relation,$\rho_{A,0} = 2\rho_{A,\pm1}$. Magnetic properties of the superfluid and the insulating phases are given in the 26(d) where we plot Nematic order parameter $Q^{z,z}_{A(B)}$ and singlet pair density $\rho^{SD}_{A(B)}$. We find that there is no singlet formation since $\rho^{SD}_A = \rho^{SD}_B = 0$ due to non-formation of spin pairs in ferromagnetic systems. In the$\rho = \frac{1}{2}$ density wave insulator, A-sublattice is in the nematic phase. In $\rho = \frac{1}{2}$ density wave insulator, the sublattice boson densities are $(\rho_A, \rho_B) = (1, 0)$. In this phase we find $Q^{z,z}_A > 0, Q^{z,z}_B = 0$. The behaviour of nematic order parameter is directly dependent on the density at the respective site. We present the results for Rényi EE in 27. In general, we find $S_2[A] = S_2[B]$ and are very small implying the system not being highly entangled. $S_2$ is constant in insulating phases and vary with chemical potential

in superfluid phases.

We plot the phase diagram of model 10 for $\delta$= 6 and 10 in 28(a) and (b) respectively. There are four insulating phases represented by lobes. The dotted lines represent phase diagram for $\delta$= 0 where there are only two lobes correspond to $\rho$ =1 and 2 Mott insulator phases. As we introduce the superlattice potential, these two Mott phases shrink and two additional density wave insulating phases form with average density $\rho = \frac{1}{2}$ and $\frac{3}{2}$. We also observed that these density wave insulator lobes enlarge with superlattice potential.

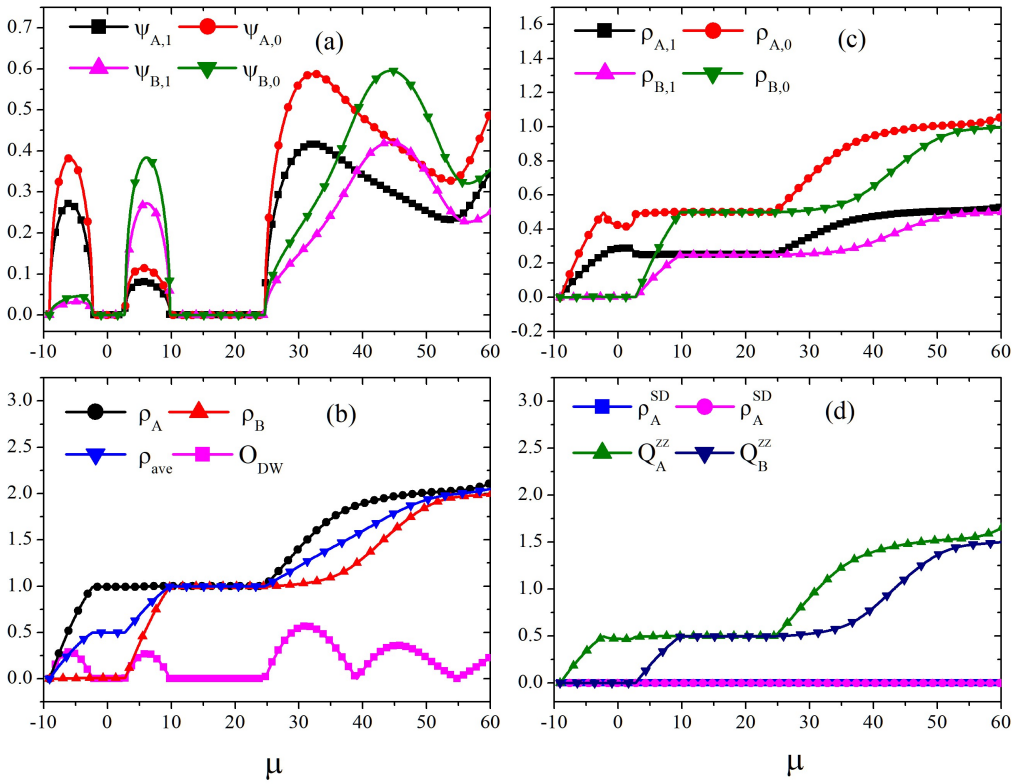


**Figure 26.** (Colour online) (a) Superfluid order parameters, (b) densities and density wave order parameters, (c) densities with spin component $\sigma$ and (d) nematic order and singlet pair density are plotted as a function of chemical potential $\mu$ for $U_0$ = 39, $U_2$ = -0.03$U_0$ and $\delta$ = 6.

### *3.6. Conclusion*

In our present work, we use the cluster mean field theory to study the behavior of spin-1 bosons in the optical superlattices. Since intra-site fluctuations are treated exactly in CMFT, it permits us to study the magnetic and the superfluid properties of the system simultaneously. Our investigation primarily focused on the ferromagnetic case ($U_2 < 0$). We conclude that, in bi-chromatic superlattices, the introduction of superlattice potential favours the localisation of the bosons and this leads to density wave Mott insulators. When $\delta$=0, we have uniform superfluid and Mott insulator phases. As

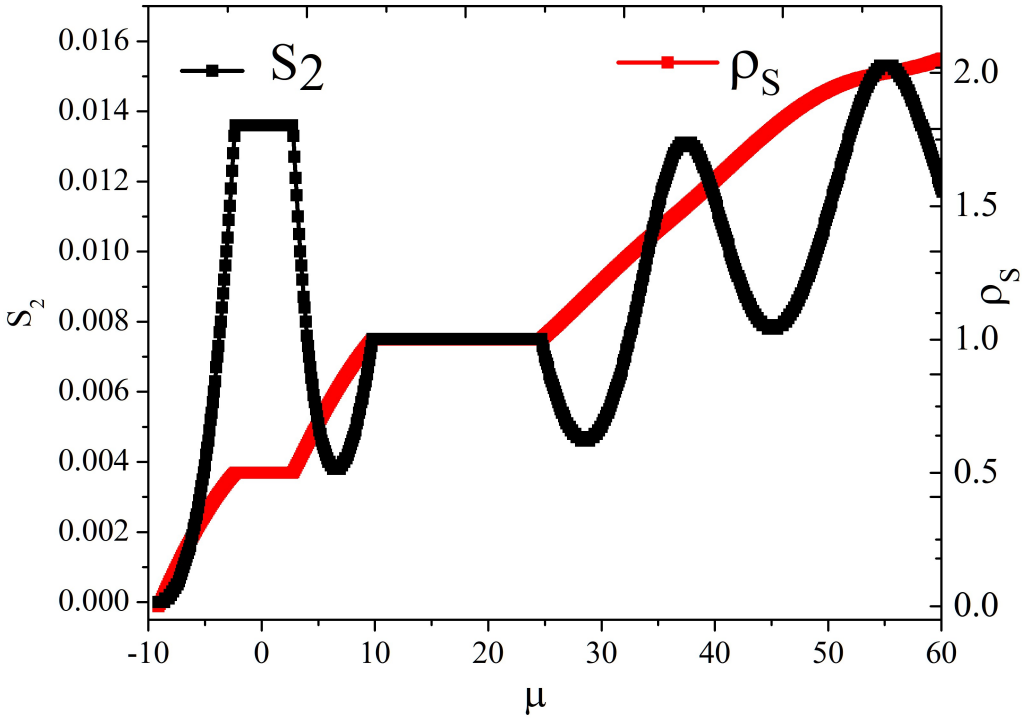


**Figure 27.** (Colour online) RényiEE $S_2$ and superfluid density $\rho_S$ are plotted as a function of chemical potential $\mu$ for $U_0 = 39$, $U_2 = -0.03U_0$ and $\delta = 6$.

$\delta$ increases, the uniform Mott insulator lobes shrink while the half integer density wave insulator lobes enlarge. The symmetry of the superfluid phase remains unaffected by the superlattice potential. We have also studied the magnetic properties of insulating phases as well as calculated Rényi EE. We notice the absence of singlet phases. The magnetic property of the density wave insulator, however, depends on the sub-lattice density. Rényi EE remains mostly small.

## References

[1] Ho T L 1998 *Phys. Rev. Lett.* **81**(4) 742–745 URL https://link.aps.org/doi/10.1103/PhysRevLett.81.742

[2] Demler E and Zhou F 2002 *Phys. Rev. Lett.* **88**(16) 163001 URL https://link.aps.org/doi/10.1103/PhysRevLett.88.163001

[3] Pai R V, Sheshadri K and Pandit R 2008 *Phys. Rev. B* **77**(1) 014503 URL https://link.aps.org/doi/10.1103/PhysRevB.77.014503

[4] Toga Y, Tsuchiura H, Yamashita M, Inaba K and Yokoyama H 2012 *Phys. Soc. Jpn.* **81**

[5] Imambekov A, Lukin M and Demler E 2003 *Phys. Rev. A* **68**(6) 063602 URL https://link.aps.org/doi/10.1103/PhysRevA.68.063602

[6] Katsura H and Tasaki H 2013 *Phys. Rev. Lett.* **110**(13) 130405 URL https://link.aps.org/doi/10.1103/PhysRevLett.110.130405

[7] Rizzi M, Rossini D, De Chiara G, Montangero S and Fazio R 2005 *Phys. Rev. Lett.* **95**(24) 240404

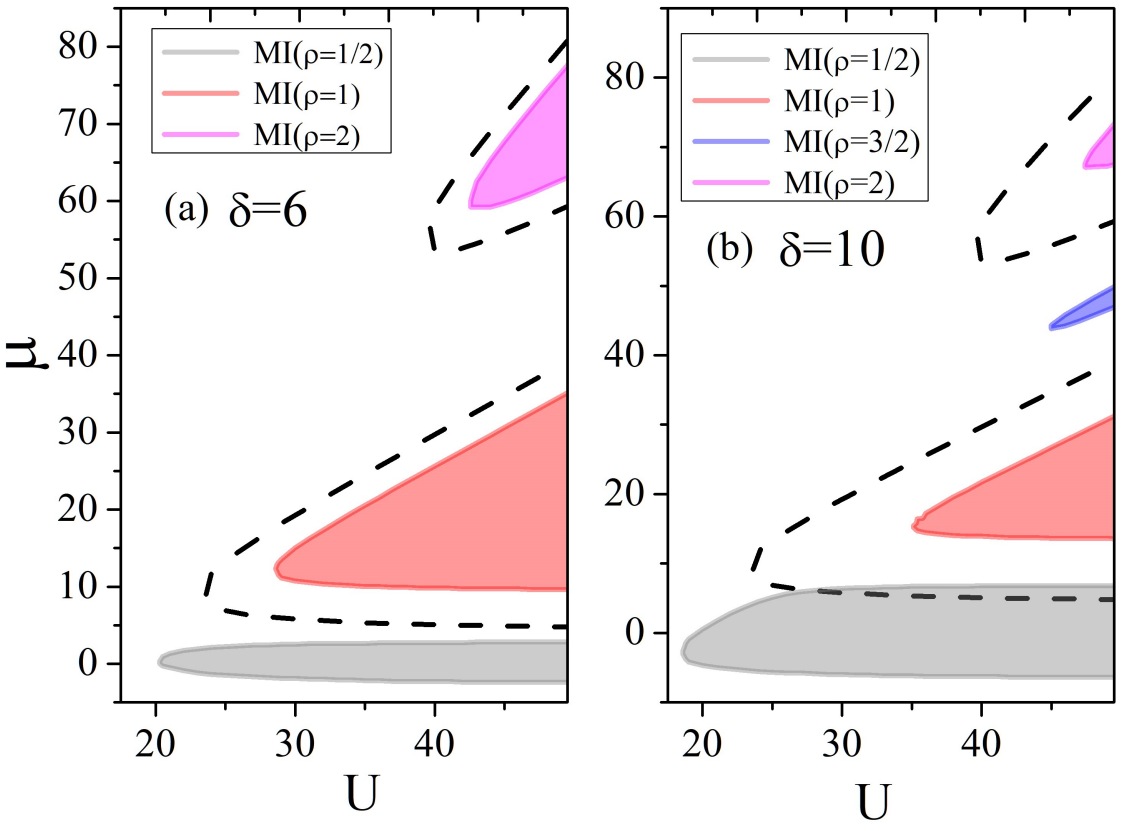


**Figure 28.** (Colour online) Phase diagram of model (1) for (a)$\delta = 6$ and (b) $\delta = 10$. The coloured lobes are insulating phases and rest of the region is polar superfluid. The dashed line represent the phase diagram for $\delta = 0$.

URL https://link.aps.org/doi/10.1103/PhysRevLett.95.240404

[8] Bergkvist S, McCulloch I P and Rosengren A 2006 *Phys. Rev. A* **74**(5) 053419 URL https://link.aps.org/doi/10.1103/PhysRevA.74.053419

[9] Apaja V and Syljuåsen O F 2006 *Phys. Rev. A* **74**(3) 035601 URL https://link.aps.org/doi/10.1103/PhysRevA.74.035601

[10] de Forges de Parny L, Hébert F, Rousseau V G and Batrouni G G 2013 *Phys. Rev. B* **88**(10) 104509 URL https://link.aps.org/doi/10.1103/PhysRevB.88.104509

[11] Horodecki R, Horodecki P, Horodecki M and Horodecki K 2009 *Rev. Mod. Phys.* **81**(2) 865–942 URL https://link.aps.org/doi/10.1103/RevModPhys.81.865

[12] Bennett C H, Bernstein H J, Popescu S and Schumacher B 1996 *Phys. Rev. A* **53**(4) 2046–2052 URL https://link.aps.org/doi/10.1103/PhysRevA.53.2046

[13] Giorda P and Zanardi P 2004 *EPL (Europhysics Letters)* **68** 163 URL http://stacks.iop.org/0295-5075/68/i=2/a=163

[14] Buonsante P and Vezzani A 2007 *Phys. Rev. Lett.* **98**(11) 110601 URL https://link.aps.org/doi/10.1103/PhysRevLett.98.110601

[15] Luchli A M and Kollath C 2008 *J. Stat. Mech* **2008** P05018 URL http://stacks.iop.org/1742-5468/2008/i=05/a=P05018

[16] Alba V, Haque M and Läuchli A M 2013 *Phys. Rev. Lett.* **110**(26) 260403 URL https://link.aps.org/doi/10.1103/PhysRevLett.110.260403

[17] Pino M, Prior J, Somoza A M, Jaksch D and Clark S R 2012 *Phys. Rev. A* **86**(2) 023631 URL https://link.aps.org/doi/10.1103/PhysRevA.86.023631

[18] Frérot I and Roscilde T 2016 *Phys. Rev. Lett.* **116**(19) 190401 URL https://link.aps.org/doi/10.1103/PhysRevLett.116.190401

[19] Isakov S V, Hastings M B and Melko R G 2011 *Nat Phys* **7** 772–775 ISSN 1745-2473 URL http://dx.doi.org/10.1038/nphys2036

[20] Zhang L, Qin X, Ke Y and Lee C 2016 *Phys. Rev. A* **94**(2) 023634 URL https://link.aps.org/doi/10.1103/PhysRevA.94.023634

[21] McIntosh T, Pisarski P, Gooding R J and Zaremba E 2012 *Phys. Rev. A* **86**(1) 013623 URL https://link.aps.org/doi/10.1103/PhysRevA.86.013623

[22] Singh M, Mishra T, Pai R V and Das B P 2014 *Phys. Rev. A* **90**(1) 013625 URL https://link.aps.org/doi/10.1103/PhysRevA.90.013625

[23] Islam R, Ma R, Preiss P M, Eric Tai M, Lukin A, Rispoli M and Greiner M 2015 *Nature* **528** 77–83 ISSN 0028-0836 article URL http://dx.doi.org/10.1038/nature15750

[24] Jaksch D, Bruder C, Cirac J I, Gardiner C W and Zoller P 1998 *Phys. Rev. Lett.* **81**(15) 3108–3111 URL https://link.aps.org/doi/10.1103/PhysRevLett.81.3108

[25] Bloch I, Dalibard J and Zwerger W 2008 *Rev. Mod. Phys.* **80**(3) 885–964 URL https://link.aps.org/doi/10.1103/RevModPhys.80.885

[26] Bloch I 2005 *Nature Physics* **1**

[27] Greiner M, Mandel O, Esslinger T, Hänsch T W and Bloch I 2002 *Nature* **415** 39 EP – article URL http://dx.doi.org/10.1038/415039a

[28] Dhar A, Singh M, Pai R V and Das B P 2011 *Phys. Rev. A* **84**(3) 033631 URL https://link.aps.org/doi/10.1103/PhysRevA.84.033631

[29] Alavani B K, Das A and Pai R V 2018 *Journal of Physics B: Atomic, Molecular and Optical Physics* **51** 145302 URL http://stacks.iop.org/0953-4075/51/i=14/a=145302

# Spectral weight of excitations in Bose Hubbard model

Bhargav K. Alavani and Ramesh V. Pai

Citation: AIP Conference Proceedings **1832**, 030009 (2017); doi: 10.1063/1.4980188
View online: http://dx.doi.org/10.1063/1.4980188
View Table of Contents: http://aip.scitation.org/toc/apc/1832/1
Published by the American Institute of Physics

# Spectral Weight Of Excitations In Bose Hubbard Model

Bhargav K. Alavani and Ramesh V. Pai

*Department of Physics, Goa University, Taleigao Plateau, Goa 403 206, India*
*E-mail: physics.bhargav@unigoa.ac.in*

**Abstract.** We obtain excitation spectra in the superfluid and the Mott Insulator phases of Bose Hubbard model near unit filling within Random Phase Approximation (RPA) and calculate its spectral weight. This gives a transparent description of contribution of each excitation towards the total Density of States (DOS) which we calculate from these spectral weights.

**Keywords:** Bose Hubbard Model, Phase transitions, Excitations.
**PACS:** 67.85.De, 03.75.Kk, 05.30.Jp

## INTRODUCTION

Great control and flexibility over ultracold gases loaded in optical lattice has led itself as a important tool to study quantum phase transitions in precise way [1]. Bosonic gases in such lattice are described by Bose-Hubbard Models, which predicts many novel phases including much studied superfluid (SF) and Mott-insulating (MI) phases. These models have received great interest ever since proposal and experimental realization of Bose Hubbard model [2,3]. Varity of theoretical techniques like Quantum Monte Carlo, DMRG, mean field theory have been employed to study its phase diagram and excitations. These are in good agreement with each other.

Although great amount of work has been done on calculating excitations and density of states (DOS) of these excitations for this model, a proper description of spectral weight of each excitation and its contribution towards DOS is lacking. In this letter we obtain excitations within Random Phase Approximation (RPA) within mean felid theory of Bose Hubbard Model and calculate the spectral weight for each of them. Further we calculate Density of States corresponding to each of these excitations. In next section we give model and method of calculation. In final section we present the results obtained**.**

## MODEL AND METHOD

Model describing bosons in optical lattice is given by

$$H = -t\sum_{\langle i,j\rangle}(a_i^{+}a_j + h.c) + \frac{U}{2}\sum_i \hat{n}_i(\hat{n}_i - 1) - \mu\sum_i \hat{n}_i \qquad (1)$$

where $t$ is the hopping amplitude and summation $<i,j>$ runs over all the nearest neighboring sites. $a^{+}_i(a_i)$ and $n_i$ are, respectively, the boson creation (annihilation) and number operators at site $i$. $U$ is the onsite repulsion strength and $\mu$ is chemical potential.

### Mean Field Theory

Hamiltonian (1) can be solved by using mean field approximation which reduces the full Hamiltonian into summation over single site Hamiltonian [4]. This is done by writing creation (annihilation) operators as a average value and fluctuations, i.e. $a_i=<a_i>+\delta a_i$ ($a^{+}_i=<a^{+}_i>+\delta a^{+}_i$). Introducing superfluid order parameter $\psi=<a_i>$, Hamiltonian (1) can be re-written as $H = \sum_i H_i^{MF} - t\sum_{<ij>}(\delta a_i^{+}\delta a_j + H.C)$ where

$$H_i^{MF} = -zt(a_i^{+} + a_i)\psi + \frac{U}{2}n_i(n_i - 1) - \mu\, n_i + zt\psi^2$$

and $z$ is the coordination number of the lattice. We scale all parameters by setting $zt=1$. Mean field Hamiltonian is solved by operating it on number basis $|0>,|1>...|n_{max}>$ and calculating $\psi$ self-consistently. Here $n_{max}$ is maximum number of bosons allowed per site to truncate the single site Hilbert space and it depends on onsite interaction $U$ and $\mu$. This gives us eigen energies $E_\alpha$ and eigen states $|i\alpha>$ of the single site Hamiltonian. The boson density $\rho=<n_i>$ is calculated from the ground state. Non-zero order parameter $\psi$ shows a superfluid phase whereas vanishing order parameter with integer ρ predicts Mott insulating phase. Phase diagram is plotted in Figure (1) where we focused near density $\rho=1$.

*DAE Solid State Physics Symposium 2016*
AIP Conf. Proc. 1832, 030009-1–030009-3; doi: 10.1063/1.4980188
Published by AIP Publishing. 978-0-7354-1500-3/$30.00

## Excitations within Random Phase Approximations

The excitations are obtained from the single particle Green's Function defined by $g_{i,j}(t) = -i\theta(t)\langle[a_i(t), a^+{}_j(0)]\rangle$ where $\theta(t)$ is Heaviside step function. We construct standard basis operator [5] using the mean field states; we define $L^i_{\alpha\alpha'}=|i\alpha><i\alpha'|$. The single particle Green's function can be written as $g_{i,j}(t) = \sum_{\alpha\alpha'\beta\beta'} T^{ij}_{\alpha\alpha'\beta\beta'} G^{ij}_{\alpha\alpha'\beta\beta'}(t,)$ where $T^{ij}_{\alpha\alpha'\beta\beta'}=<i\alpha|a^+{}_i|i\alpha'><j\beta|a_j|\beta'>$ and $G^{ij}_{\alpha\alpha'\beta\beta'}(t) = -i\theta(t)\langle[L^i_{\alpha\alpha'}(t), L^j_{\beta\beta'}(0)]\rangle$. We solve equation of motion for $G^{ij}{}_{\alpha\alpha'\beta\beta'}$ within Random Phase Approximation and Fourier transforming it into momentum and energy space, we get

$$(\omega - E_\alpha + E_{\alpha'})G_{\alpha\alpha'\beta\beta'}(k,\omega) = \frac{1}{2\pi}P_{\alpha\alpha'}\delta_{\alpha\beta'}\delta_{\beta\alpha'} + \varepsilon_k P_{\alpha\alpha'}\sum_{\mu\nu}\breve{T}_{\alpha\alpha'\nu\mu}G_{\mu\nu\beta\beta'}(k,\omega)$$

where $P_{\alpha\alpha'}=< L_{\alpha\alpha}>-< L_{\alpha'\alpha'}>$, $\breve{T}_{\alpha\alpha'\beta\beta'}= T_{\alpha\alpha'\beta\beta'}+ T_{\beta\beta'\alpha\alpha'}$ and $\varepsilon_k = -\frac{1}{3}\sum_{j=x,y,z}\cos(\pi k_j)$

Solving the equation of motion for the Green function and writing it in the form

$$g_{\alpha\alpha'\beta\beta'}(k,\omega) = \sum_i \frac{A_i'(k)}{\omega - \omega_i(k)} \qquad (2)$$

we get excitation spectra $\omega_i(k)$ and its spectral weights $A'_i(k)$. Summation $i$ runs for all excitations. Density of states for each excitation $\omega_i(k)$ is calculated by $N_i(\omega) = -\frac{1}{\pi}\sum_k \mathrm{Im}[g_i(k,\omega^+)]$ where $\omega^+ = \omega + i\delta$; we have added small complex part to ω. Results of these calculations have been shown in the next section.

## RESULTS

The phase diagram of model (1) near unit density is shown in Figure (1). We choose few characteristic points shown in the figure by red dots to obtain the excitations. For example excitations at point (a) (density ρ=0.5) in Figure (1) are plotted in the Figure (2). Here we choose $k_y=k_z=0$ and plot excitations as function of $k_x$. First particle (green line) and hole (blue line) excitations are gapless consistent with the SF nature of the phase. The first gapped particle (red line) excitation has finite weight, however first gapped hole (orange line) excitation has almost zero weight. This is because for ρ=0.5 it is easy to create particle excitation than hole excitation. In all cases we see that spectral weights for excitations near to $k_x$=0 are dominant and it reduces as we increase $k_x$. We have not shown particle and hole excitations which have zero spectral weights.

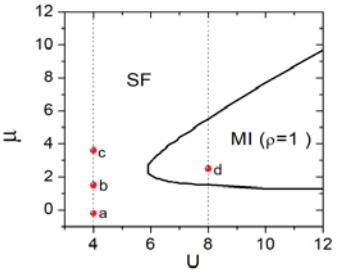


**FIGURE 1.** Mean field phase diagram of model (1) near unit density. Red dots are the points where excitations are calculated and presented below.

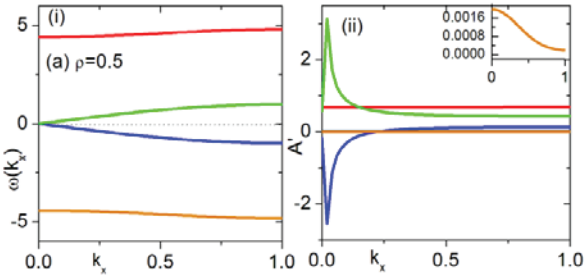


**FIGURE 2.** (i) Excitation spectra for point (a) in figure (1). (ii) represents corresponding spectral weights. Excitation and corresponding spectral weight are represented by same coloured line. (inset) Weight for lowest hole excitation.

Density of States (DOS) for each of these excitations, using the same colour coding, is plotted in figure (3).

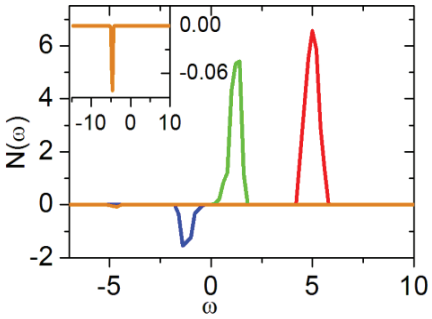


**FIGURE 3.** DOS of excitations of figure (2).

Similar plots for points (b) (with ρ=1.04) and (c) (ρ=1.5) are given in figure (4). As we increase the density, but continue to be in the SF phase, several higher excitations contributes to the DOS since the spectral weight of these excitations are finite. Both particle and hole excitations contributes significantly.

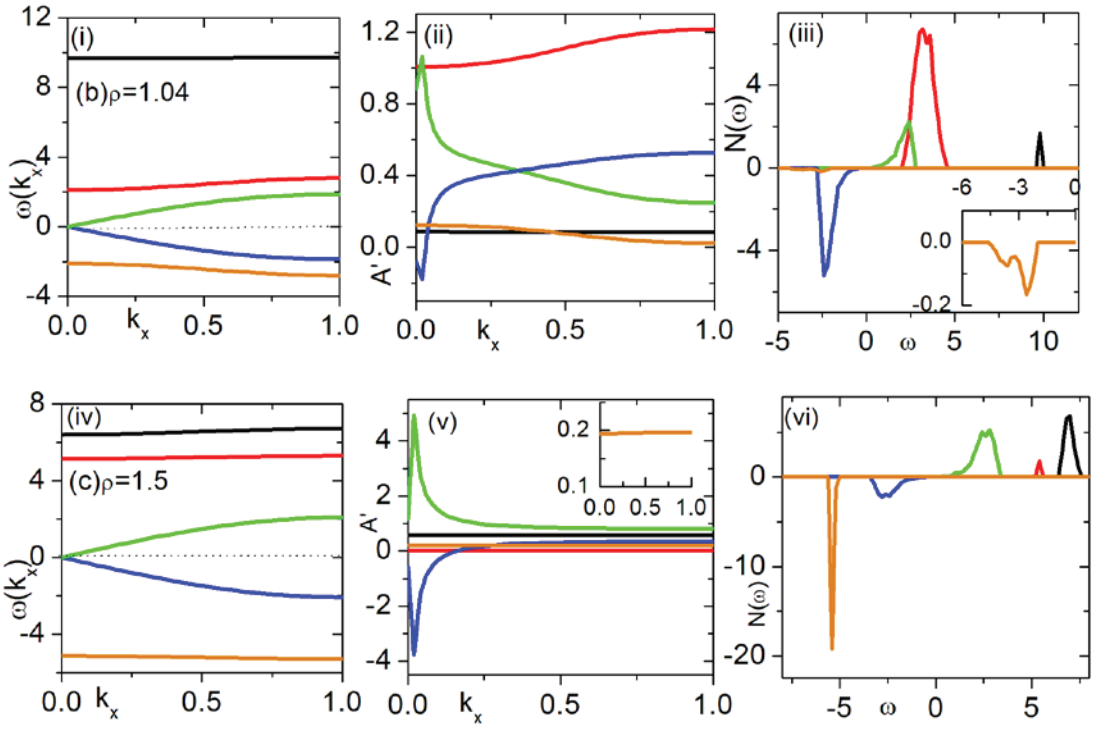


**FIGURE 4.** Excitations (i) and (iv), their spectral weights (ii) and (v) and DOS (iii) and (vi), respectively, for density ρ=1.04 (point (b) in figure (1)) and ρ=1.5 (points (c) in figure (1)).

For Mott insulator, near the lower edge of lobe (point (d)), the excitations and their weights are given in figure (5). Both particle and hole excitations have finite gap. Hole excitation has smaller gap compare to particle excitation. Since the point we choose is closer to the lower edge of the lobe, the hole excitation has higher spectral weight. The corresponding density of state is given in figure (6).

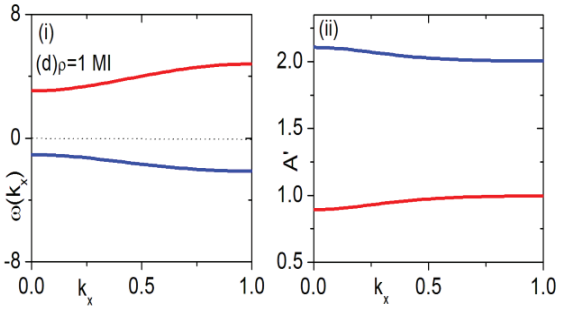


**FIGURE 5.** Excitations (i) and weights (ii) for point (d) in figure (1). Only excitations which have finite spectral weight have shown here.

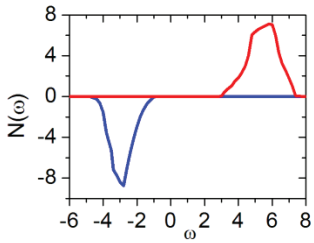


**FIGURE 6.** DOS of excitations of figure (5) in MI phase.

## ACKNOWLEDGMENTS

This work is supported by CSIR grant No. 03(1306)/14/EMR-II. BKA acknowledges UGC-BSR fellowship.

## REFERENCES

1. I. Bloch *et al. Rev. Mod. Phys.* **80** 885 (2008).
2. M. Greiner *et al. Nature* **415** 39 (2002).
3 D. Jaksch, *et al. Phys. Rev. Lett.* **81** 3108 (1998).
4. K. Sheshadri *et al. EPL*, **22** 257 (1993).
5. Stephen B. Haley *et al*. *Phys. Rev. B*, **5** 3 (1972).

# Spin-1 bosons in optical superlattice

Cite as: AIP Conference Proceedings **2115**, 030016 (2019); https://doi.org/10.1063/1.5112855
Published Online: 12 July 2019

Chetana G. F. Gaonker, B. K. Alavani, A. Das, and R. V. Pai

# Spin-1 Bosons in optical superlattice

Chetana G.F. Gaonker[1,a)], B. K. Alavani[1], A. Das[2] and R. V. Pai[1]

[1]*Department of Physics, Goa University, Taleigao Plateau, Goa 403206*
[2]*Department of Physics, Parvatibai Chowgule College of Arts and Science, Gogol, Margao, Goa 403602*

[a)] physics.chetana@unigoa.ac.in

**Abstract.** In this paper, we analyze superfluid, insulator and various magnetic phases of ultracold spin-1 bosonic atoms in two-dimensional optical superlattices. Our studies have been performed using Cluster Mean Field Theory. Calculations have been carried out for a wide range of densities and the energy shifts due to the superlattice potential. We find superlattice potential do not change the symmetry of the polar superfluid phases. Superlattice potentials induce Mott insulator phases with half-integer densities. The phase diagram is obtained using superfluid density, nematic order and singlet density. Second order Rényi entanglement entropy is also calculated in different phases. The results show that Rényi entanglement entropy is large in the nematic Mott insulator phase.

## INTRODUCTION

Ultracold atoms in optical lattices and superlattices provide us with the realization of engineered quantum many-body lattice models [1]. One remarkable development in this context is the realization of Bose gases in the optical lattices. Superfluid (SF) to Mott Insulator (MI) quantum phase transition in cold bosonic atoms has received great scientific attention since its theoretical prediction in the context of Bose Hubbard model (BHM), and followed by its experimental realization [2-4]. When traps are purely optical, Alkali atoms like $^{87}$Rb, $^{23}$Na and $^{30}$K, with hyperfine spin F=1, have spin degrees of freedom and thus, the interaction between bosons is spin-dependent [5]. The interaction is ferromagnetic (e.g. $^{87}$Rb) or anti-ferromagnetic (e.g. $^{23}$Na), depending upon scattering lengths of singlet and quintuplet channels [6]. The spin-dependent interaction in spinor gases exhibits richer quantum effects than their single-component counterparts and it not only modifies the nature of phase diagrams but also allows the study of superfluidity and magnetism.

The optical superlattices are obtained by super-imposition of two monochromatic lattices with slightly different wavelengths [7]. Manipulating the relative phase between the two standing waves and their respective depths independently, a periodic pattern of potential wells with two different depths at two adjacent sites is obtained. This difference in the depth of two adjacent sites is the measure of superlattice potential. In this report, we investigate spin-1 ultracold bosons loaded into 2-dimensional bi-chromatic optical superlattices.

## MODEL AND METHOD

The spin-1 Bose–Hubbard model, which describes spin full bosons in an optical superlattice, is given by

$$\mathcal{H} = -t \sum_{\langle i,j\rangle,\sigma}\left(a_{i,\sigma}^{\dagger}a_{j,\sigma} + a_{j,\sigma}^{\dagger}a_{i,\sigma}\right) + \frac{U_0}{2}\sum_i \hat{n}_i(\hat{n}_i - 1) + \frac{U_2}{2}\sum_i(\vec{F}_i^2 - 2\hat{n}_i) - \sum_i \mu_i \hat{n}_i, \quad (1)$$

where first term represents hopping of bosons between nearest neighbour sites $\langle i,j\rangle$ with an amplitude $t$. Here $a_{i,\sigma}$ ($a_{i,\sigma}^{\dagger}$) represents annihilation (creation) operator at site $i$ with spin projection $\sigma = \{-1, 0, 1\}$, number operator $\hat{n}_{i,\sigma} = a_{i,\sigma}^{\dagger}a_{i,\sigma}$ and $\hat{n}_i = \sum_\sigma \hat{n}_{i,\sigma}$. Spin operator $\vec{F}_i = \left(F_i^x, F_i^y, F_i^z\right)$ where $F_i^\alpha = \sum_{\sigma,\sigma'} a_{i,\sigma}^{\dagger} S_{\sigma,\sigma'}^{\alpha} a_{i,\sigma'}$ with $\alpha = x, y, z$ and $S_{\sigma,\sigma'}^{\alpha}$ are standard spin-1 matrices. Spin independent (dependent) interaction $U_0(U_2)$ arises due to the difference in the scattering length $a_0$ and $a_2$ in the spin S=0 and S=2 channels respectively. The spin dependent interaction $U_2$ can be positive (anti-ferromagnetic) or negative (ferromagnetic) depending on the values of $a_0$ and $a_2$ [5]. The site dependent chemical potential $\mu_i = \mu + (-1)^i\delta$ where $\mu$ controls the bosons density and $\delta$ is the shift in energy due to superlattice potential. Here, we consider a bi-chromatic superlattice and thus, the whole lattice is bipartite into A and B sub-lattices with $\mu_A = \mu + \delta$ and $\mu_B = \mu - \delta$.

*DAE Solid State Physics Symposium 2018*
AIP Conf. Proc. 2115, 030016-1–030016-4; https://doi.org/10.1063/1.5112855
Published by AIP Publishing. 978-0-7354-1851-6/$30.00

In the cluster mean-field theory [8], the entire lattice is divided into clusters with $N_C$ number of sites. In this calculation we take $N_C = 2$ and thus, each cluster consists of one site each from A and B sub-lattices. Decoupling each cluster from its nearest neighbor clusters using standard mean-field procedure [6,8,9], the model (1) is given by

$$\mathcal{H} = \sum_{clusters} \mathcal{H}^C$$

$$\mathcal{H}^C = -t\sum_{\sigma}\left(a^{\dagger}_{A,\sigma}a_{B,\sigma} + a^{\dagger}_{B,\sigma}a_{A,\sigma}\right) - 3t\sum_{\sigma}\left[\left(a^{\dagger}_{A,\sigma} + a_{A,\sigma}\right)\psi_{B,\sigma} + \left(a^{\dagger}_{B,\sigma} + a_{B,\sigma}\right)\psi_{A,\sigma} - 2\psi_{A,\sigma}\psi_{B,\sigma}\right]$$
$$+\frac{U_0}{2}\sum_{i=A,B}\hat{n}_i(\hat{n}_i - 1) + \frac{U_2}{2}\sum_{i=A,B}(\vec{F}_i^2 - 2\hat{n}_i) - \sum_{\sigma}\left(\mu_A\hat{n}_{A,\sigma} + \mu_B\hat{n}_{B,\sigma}\right). \quad (2)$$

Here $\psi_{A,\sigma} = \langle a_{A,\sigma}\rangle$ $\left(\psi_{B,\sigma} = \langle a_{B,\sigma}\rangle\right)$ is the A (B) sub-lattice superfluid order parameter with spin component $\sigma$. We determine $\psi_{A,\sigma}$ and $\psi_{B,\sigma}$ self-consistently using the method described in Ref. [8]. Sub-lattice superfluid densities $\rho^S_{A(B)} = \sum_{\sigma}\left|\psi_{A(B),\sigma}\right|^2$ and densities of bosons $\rho_{A(B)} = \langle\hat{n}_{A(B)}\rangle$ are calculated from this self-consistently determined ground state. We also calculate the average density of bosons $\rho = \frac{1}{2}(\rho_A + \rho_B)$ and the density wave order parameter $O_{DW} = |\rho_A - \rho_B|$. We can characterize the ground state of model (1) from these quantities. The ground state is a superfluid (Mott insulator) if $\rho^S_{A(B)}$ is non-zero (zero). The magnetic properties of the superfluid and Mott insulator phases are determined from Nematic order parameter $Q^{\alpha,\alpha}_{A(B)} = \langle\left(F^{\alpha}_{A(B)}F^{\alpha}_{A(B)} - \frac{1}{3}\langle\vec{F}^2_{A(B)}\rangle\right)\rangle$[10] and singlet pair density $\rho^{SD}_{A(B)} = \langle\hat{A}^{\dagger}_{A(B)}\hat{A}_{A(B)}\rangle$, where the singlet creation operator $\hat{A}^{\dagger}_{A(B)} = \left(2a^{\dagger}_{A(B),1}a^{\dagger}_{A(B),-1} - a^{\dagger}_{A(B),0}a^{\dagger}_{A(B),0}\right)$. In addition to these quantities, we also investigate entanglement properties [10] of different ground states by calculating Rényi entanglement entropy (EE) [11] given by $S_2[A(B)] = -log\left(Tr\left(\rho^2_{A(B)}\right)\right)$ where $\rho_{A(B)}$ is the reduced density matrix for sub-lattice A (B).

## RESULTS

We now present the results of the Cluster Mean Field Theory applied to 2-dimensional spin-1 Bose Hubbard model in bi-chromatic superlattice, with cluster size $N_C = 2$. Here we restrict ourselves to the anti-ferromagnetic case $U_2 > 0$. We set our energy scale by choosing *t=1* and thus all parameters are dimensionless. It is known from the earlier studies that, for the anti-ferromagnetic case ($U_2 > 0$), the symmetry the superfluid phase is polar (PSF) [8] and in the mean-field level symmetry restricts values of the superfluid order parameters such that either $\psi_{A(B),1} = \psi_{A(B),-1} \neq 0$, $\psi_{A(B),0} = 0$ or $\psi_{A(B),1} = \psi_{A(B),-1} = 0$ and $\psi_{A(B),0} \neq 0$ [8]. Superfluid order parameters are plotted in the Fig. 1(a) for $U_0 = 30$, $U_2 = 0.03U_0$ and superlattice potential $\delta = 6$. It is evident from the Fig. 1(a) that the superfluid phases have polar symmetry: we find $\psi_{A(B),1} = \psi_{A(B),-1} \neq 0$ and $\psi_{A(B),0} = 0$ and thus, superlattice potential do not change this symmetry. There are four regions in the chemical potentials where $\psi_{A(B),\sigma} = 0$ thus, correspond to four insulator phases. The sublattice bosons densities $\rho_A$ and $\rho_B$, the average boson density $\varrho = \frac{1}{2}(\rho_A + \rho_B)$ and the density wave order parameter $O_{DW}$ are plotted in the Fig. 1(b). The four insulator regions have average densities $\rho = \frac{1}{2}, 1, \frac{3}{2}$ and 2 with sublattice densities $(\rho_A, \rho_B) = (1,0), (1,1), (2,1)$ and (2, 2), respectively. Insulators with the density $\rho = 1$ and 2 are the normal Mott insulators where the density is uniform across whole lattice and $O_{DW} = 0$. However, insulators with $\rho = \frac{1}{2}$ and $\frac{3}{2}$ have finite $O_{DW}$ and are called density wave insulators. Thus, the superlattice potential introduces additional insulator phases with half-integer bosons densities. The sublattice bosons densities with different spin component $\rho_{A(B),\sigma}$ are plotted in the Fig. 1(c). In general, we find $\rho_{A(B),\pm1} > \rho_{(A,B),0}$ except in the Mott insulator region, i.e., for $\rho = 1$ and 2, we find $\rho_{A,\pm1} = \rho_{A,0} = \rho_{B,\pm1} = \rho_{B,0}$. It should be noted here that the symmetry of the polar superfluid phase is such that $\psi_{A(B),1} = \psi_{A(B),-1} \neq 0$ and $\psi_{A(B),0} = 0$. This imply that the bosons with spin component $\sigma = 0$, though present in the system are not in the superfluid phase. Only bosons with spin component $\sigma = \pm1$ form superfluid. This leads to a situation where we have a two-fluid model with bosons with $\sigma = \pm1$ are in superfluid phase while bosons with $\sigma = 0$ are in the normal fluid phase. Magnetic properties of the superfluid and the insulating phases are given in the Fig. 1(d) where we plot Nematic order parameter $Q^{z,z}_{A(B)}$ and singlet pair density $\rho^{SD}_{A(B)}$. We find that density $\rho = 2$ Mott insulator phase is a singlet phase with $\rho^{SD}_A = \rho^{SD}_B = 1$ and $Q^{z,z}_A = Q^{z,z}_B = 0$. The density $\rho = 1$ Mott insulator phase, however, is nematic $Q^{z,z}_A = Q^{z,z}_B > 0$ and $\rho^{SD}_A = \rho^{SD}_B = 0$. In

$\rho = \frac{1}{2}$ density wave insulator, the sublattice boson densities are $(\rho_A, \rho_B) = (1,0)$. In this phase we find $Q_A^{z,z} > 0$, $Q_B^{z,z} = 0$ and $\rho_A^{SD} = \rho_B^{SD} = 0$. In the $\rho = \frac{3}{2}$ density wave insulator, however, $Q_B^{z,z} > 0$, $Q_A^{z,z} = 0$ and $\rho_A^{SD} = 1$, $\rho_B^{SD} = 0$. So, in the $\rho = \frac{3}{2}$ density wave insulator, A-sublattice is in the singlet phase and B-sublattice is in the nematic phase, whereas in the $\rho = \frac{1}{2}$ density wave insulator, A-sublattice is in the nematic phase. We present the results for Rényi EE in Fig. 2. In general, we find $S_2[A] = S_2[B]$ and are very small except in the $\rho = 1$ Mott insulator where $S_2$ is two orders of magnitude larger. $S_2$ is constant in insulating phases and vary with chemical potential in polar superfluid phases.

We plot the phase diagram of model (1) for $\delta = 6$ and 10 in Fig. 3(a) and (b) respectively. There are four insulating phases represented by lobes. The dotted lines represent phase diagram for $\delta = 0$ where there are only two lobes correspond to $\rho = 1$ and 2 Mott insulator phases. As we introduce the superlattice potential, these two Mott phases shrink and two additional density wave insulating phases form with average density $\rho = \frac{1}{2}$ and $\frac{3}{2}$. We also observed that these density wave insulator lobes enlarge with superlattice potential.

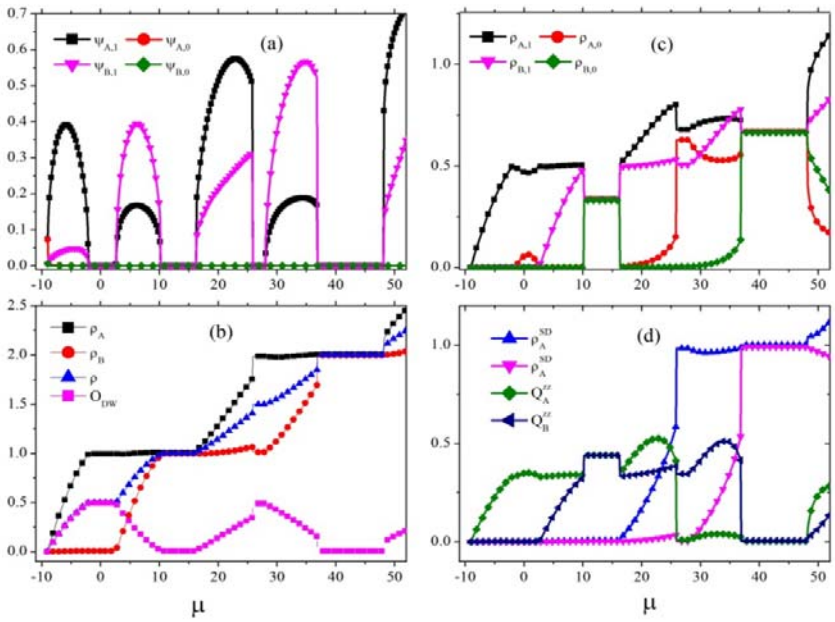


**FIGURE 1.** (Colour online) (a) Superfluid order parameters, (b) densities and density wave order parameters, (c) densities with spin component $\sigma$ and (d) nematic order and singlet pair density are plotted as a function of chemical potential μ for $U_0 = 30$, $U_2 = 0.03U_0$ and $\delta = 6$.

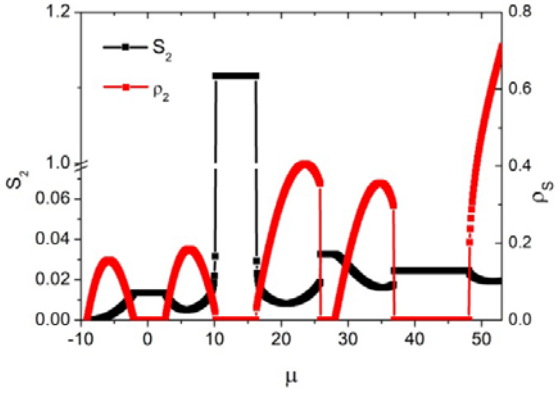


**FIGURE 2.** (Colour online) Rényi EE $S_2$ and superfluid density $\rho_S$ are plotted as a function of chemical potential μ for $U_0$=30, $U_2$=0.03$U_0$ and δ=6.

## CONCLUSION

In our present work, we use the cluster mean field theory to study the behavior of spin-1 bosons in the optical superlattices. Since intra-site fluctuations are treated exactly in CMFT, it permits us to study the magnetic and the superfluid properties of the system simultaneously. Our investigation primarily focused on the anti ferromagnetic case ($U_2 > 0$). We conclude that, in bi-chromatic superlattices, the introduction of superlattice potential favours the localisation of the bosons and this leads to density wave Mott insulators. When $\delta = 0$, we have uniform superfluid and Mott insulator phases. As $\delta$ increases, the uniform Mott insulator lobes shrink while the half integer density wave insulator lobes enlarge. The symmetry of the superfluid phase remains unaffected by the superlattice potential. We have also studied the magnetic properties of insulating phases as well as calculated Rényi EE. We found that the $\rho = 1$ Mott lobe is nematic, and $\rho = 2$ lobe a singlet. The magnetic property of the density wave insulator, however, depends on the sub-lattice density. Rényi EE remains mostly small except at density $\rho = 1$ Mott insulator and could be used as a marker of the transition.

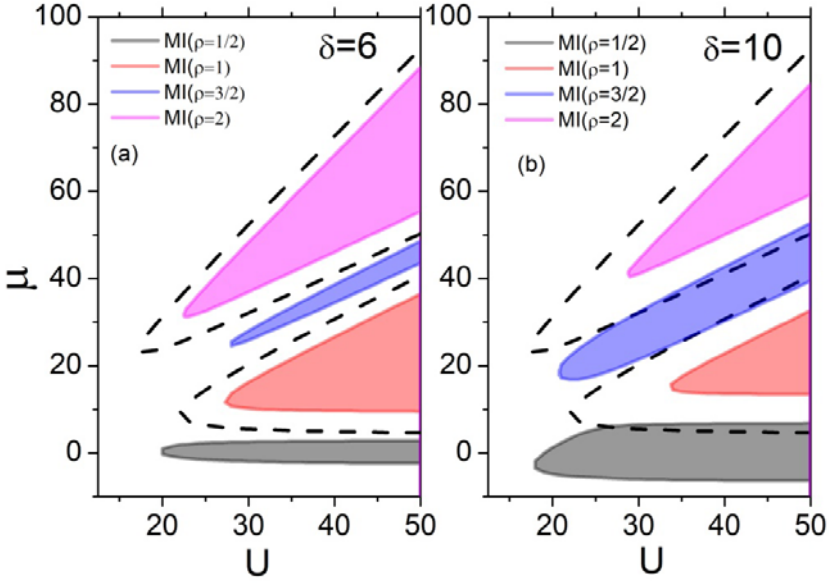


**FIGURE 3.** (Colour online) Phase diagram of model (1) for (a) $\delta = 6$ and (b) $\delta = 10$. The coloured lobes are insulating phases and rest of the region is polar superfluid. The dashed line represent the phase diagram for $\delta = 0$.

## ACKNOWLEDGMENTS

This work is supported by UGC Grant F. No. 43-520/2014/(SR) and DSTE Goa. BKA acknowledges UGC-BSR fellowship.

## REFERENCES

1. I. Bloch, J. Dalibard and W. Zwerger, Rev. Mod. Phys. **80**, 885 (2008).
2. D. Jaksch, C. Bruder, J. I. Cirac, C. W. Gardiner and P. Zoller, Phys. Rev. Lett. **81**, 3108 (1998).
3. M. Greiner, O. Mandel, T.Esslinger, T. W. Hanschand and I. Bloch, Nature **415**, 39-44 (2002).
4. I. Bloch, Nature Physics **1**, 23-30 (2005).
5. T. L. Ho, Phys. Rev. Lett. **81,** 742–5 (1998).
6. R. V. Pai, K. Sheshadri and R. Pandit, Phys. Rev. B, **77**, 014503 (2008).
7. A. Dhar, M. Singh, R. V. Pai and B. P. Das, Phys. Rev. A, **84**, 033631 (2011), M. Singh, A. Dhar, T. Mishra, R. V. Pai and B. P. Das, Phys. Rev. A, **85**, 051604(R) (2012).
8. B. K. Alavani, A. Das and R. V. Pai, J. Phys. B: At. Mol. Opt. Phys. **51** 145302 (2018).
9. T. McIntosh, P. Pisarski, R. J. Gooding and E. Zaremba Phys. Rev. A **86,** 013623 (2012).
10. R. Horodecki, P. Horodecki, M. Horodecki and K. Horodecki Rev. Mod. Phys. **81** 865–942 (2009).
11. C. H. Bennett, H. J. Bernstein, S. Popescu and B. Schumacher Phys. Rev. A **53** 2046–52 (1996).